Title: Gravity-driven structures and deposits resulting from slope collapse in the margin of a carbonate platform (Pennsylvanian, Cantabrian Zone, NW Iberia)

Author names and affiliations:

Manuel Ignacio DE PAZ-ÁLVAREZ [a,*], Juan Luis ALONSO [a], Luis Pedro FERNÁNDEZ [a]

[a] Departamento de Geología, Universidad de Oviedo, C/ Jesús Arias de Velasco s/n, 33005 Oviedo, Spain

Emails of the authors

midepaz@geol.uniovi.es; jlalonso@geol.uniovi.es; lpedro@geol.uniovi.es

Corresponding author:

Manuel Ignacio DE PAZ-ÁLVAREZ, midepaz@geol.uniovi.es, +34 985102936

Declarations of interest: none.

Keywords:

Carbonate-platform slope, Gravity-driven deformation, Slump, Thrust-related folds, Cantabrian Zone

Abstract

Lower-slope to basin-floor deposits associated to isolated microbial carbonate platforms of the Valdeteja Formation (Carboniferous foreland basin, Cantabrian Zone, NW Spain), containing large slid blocks and debrites, exhibit a combination of contractional and extensional structures, which include thrusts, backthrusts, folds, extensional faults and joints, and boudinaged beds. Several lines of evidence indicate that deformation took place in poorly lithified conditions, such as thickened hinges, hydroplastic fractures, fold axes scatter or folding of microbial limestones.

Once restored, all structures indicate a transport direction towards the NNE-ENE. This azimuth coincides with the direction towards which the thrust nappes of the southern branch of the Cantabrian Zone were emplaced during the Variscan Orogeny. However, the interpretation of the deposits and structures as gravity-related, associated to the collapse of the carbonate platform slope, is supported by features such as the rootless character of thrusts, the parallelism between transport direction and paleocurrent orientation, the concomitant development of contractional and extensional structures, the development of normal listric faults affecting the Valdeteja platform, the sedimentary environment (lower slope to basin floor) and the geological context of the Valdeteja carbonate platforms, which predate the Variscan deformation in the study area.

1. Introduction

Slump folds and faults are associated to gravitationally-driven instabilities affecting sedimentary sequences deposited on or close to a dipping surface. Their orientation is key in the identification of palaeoslope orientation in sedimentary basins (Woodcock, 1979; Strachan and Alsop, 2006; Waldron and Gagnon, 2011; Korneva *et al.*, 2016). Slump structures have been long considered chaotically arranged, but numerous papers have shown that with detailed structural studies, a consistent organization within slumped units may be found (Hanson, 1971), which allows a better understanding of slump dynamics (Farrell, 1984; Alsop and Marco, 2014) and the possibility of obtaining an estimation of the palaeoslope orientation (Woodcock, 1979; Strachan and Alsop, 2006; Alsop and Marco, 2011) from which they were generated.

The model envisioned by Farrell (1984) (see also Alsop and Marco, 2014) explains the deformation structures within a slumped unit on the basis of the existence of flow velocity variations within it, which can cause extensional and contractional 'waves' to propagate down- or upslope. The model accounts for the overprinting of previous structures and the almost synchronous development of structures with radically different kinematics (extensional and contractional) sharing common orientations, a feature commonly observed in the field (Ortner, 2007; van der Merwe *et al.*, 2011; Alsop and Marco, 2014; Korneva *et al.*, 2016; Alsop *et al.*, 2018).

The main conundrum faced during the study of gravity-driven deformation is its distinction from tectonic deformation (Ortner, 2007; Waldron and Gagnon, 2011; Korneva *et al.*, 2016; Alsop *et al.*, 2017b; 2018). Gravity-driven deformation is the result of gravitational instabilities that arise in sedimentary environments where deposits lie on a dipping surface, thus leading to slides and slumps that are translated downslope. On the contrary, tectonic deformation in a sedimentary basin is often understood as caused by lithospheric processes related to plate convergence or divergence. Of course, both deformation types can coexist in space and time, and their recognition may be impossible if no definite evidence for or against either hypothesis can be found.

Numerous key features have been provided as indicators of slumping processes. These include, among others, (i) overprinting or truncation of deformation structures by subsequent sedimentary processes; (ii) liquefaction and fluidization of unconsolidated sediment particles; (iii) fold hinge thickening, (iv) scatter of fold axial trends; (v) confinement of the structures within a particular stratigraphic interval; or (vi) synchronous development of contractional and extensional structures (Elliot and Williams, 1988; Ortner, 2007; Waldron and Gagnon, 2011; Alsop *et al*., 2017b). However, when these features fail to be found, interpretation of structures as slump-related is considerably more difficult to support (*e.g.* Waldron and Gagnon, 2011). Uncertainties at distinguishing tectonic from gravity-driven deformation mainly arise from the fact that both can lead to the same structural style and only under exceptional circumstances unequivocal criteria will develop (Maltman, 1984). Furthermore, even more complications are faced when such criteria are based on the degree of lithification of the sediment when deformation took place. It is well known that both soft and lithified sediments may deform through both gravitational and tectonic processes, and similar structures will result from either type of deformation (Ortner, 2007). Therefore, a distinction between both processes can only be accomplished through a combination of several criteria (Maltman, 1984; Waldron and Gagnon, 2011).

A key feature of gravity-driven deformation is the fact that the thrusts that bound the deformed succession are unrooted: they are not linked to a structure that cuts downwards into the stratigraphic succession, but rather to an extensional fault developed at or in close proximity to the sedimentary surface ("superficial" deformation; Waldron and Gagnon, 2011). As such, this deformation is only driven by gravity: tectonic activity (*e.g.*

earthquakes) may trigger the deformation, but the ultimate cause would be slope failure and downslope transport of sediments. Additionally, other processes, chiefly shearing by an overriding gravity flow, have been invoked in very low-gradient (~0.1°) basin floors (Dasgupta, 2008; van der Merwe *et al.*, 2011; Jablonská *et al.*, 2018). In any case, the ultimate cause of this deformation would be a downslope transport of sediments, and therefore can be considered a type of gravity-driven deformation.

The present study provides a thorough description of a variety of contractional and extensional structures developed in lower-slope to basin-floor deposits associated to a Carboniferous microbial carbonate platform developed in the Cantabrian Zone (NW Spain). The study describes overprinting patterns that resulted from sequential gravitational deformation events affecting the same poorly lithified deposits. The aim of the research is to provide arguments favouring a gravity-driven deformation, in opposition to the later Variscan tectonic deformation, which affected the Cantabrian Zone at the end of the Moscovian.

The terminology utilized in this research follows the proposed by Stow (1985), Shanmugam *et al.* (1994), Stow (1994), or Stow *et al.* (1996) for deep-marine environments, who classified gravity-related deposits in (i) slides, where strain is concentrated in a basal shear zone, with none or slight internal strain of the slid unit; (ii) slumps, where the whole unit accumulates internal strain, specially concentrated in shear zones that bound undeformed regions; and (iii) gravity flows, where pervasive internal shearing leads to the individualization of the sediment particles, which move with respect to each other in a sedimentary flow.

2. Gravity instabilities in carbonate platform slopes

Slope of carbonate platforms mostly varies according to the sediment fabric (Kenter, 1990; Kenter *et al.*, 2005). Microbial communities, which dominated the carbonate production in the Cantabrian Zone foreland basin during the Carboniferous, are known to generate massive deposits in the upper slope at water depths of up to several hundred meters, since they are not restricted to photic conditions (Della Porta *et al*., 2003; Chesnel *et al.*, 2016). Carbonate production by microbial communities is characterised by a fast cementation, which increases the internal strength of the limestones. Therefore, slope angles can reach values as high as 40°, but for the same reason the slopes are prone to collapse and avalanching (Kenter *et al.*, 2005). In contrast, lower-slope and toe-of-slope areas are dominated by bedded deposits, comprising carbonate-breccia debrites, calciturbidites and spiculitic wackestones (Della Porta *et al.*, 2003; Chesnel *et al.*, 2016). These detrital deposits may be fed mainly from: (i) the upper-slope microbial boundstones, which may be destabilized through autocyclic causes, such as an increase in the slope angle over the stability threshold, or allocyclic causes, such as earthquakes in a foreland basin; and (ii) platform-top-derived grains shed to the slope by storm activity or, again, after accumulation in a surface steeper than the angle of repose for those materials (Della Porta *et al*., 2003). The lower slope displays smaller angles, between 15° and 30°, and these decrease to less than 10° in the toe-of-slope (Della Porta *et al*., 2003; Kenter *et al*., 2005). Nevertheless, in a platform developed close to the one here studied, Chesnel *et al*. (2016) obtained lower overall slope declivities, between 10° and 22° depending on the stage of development. Under such circumstances, slope instabilities mainly involve the bedded deposits of the lower slope and toe of slope, whereas the more lithified upper-slope massive boundstones are less represented.

While the sedimentology of such deep water systems has been thoroughly described in the literature, both in the Cantabrian Zone (Bahamonde *et al*., 1988; Bahamonde y Colmenero, 1993; Bahamonde *et al*., 1997; Della Porta *et* al., 2003; Bahamonde *et al.,* 2008; Chesnel *et al.*, 2016) and elsewhere (Masetti *et al.*, 1991; Kenter, 1990; among others), gravitational collapse structures developed at carbonate platform margins have received little attention. Some recent descriptions have been provided by Alonso *et al.* (2015) for the Cantabrian Zone (NW Spain); Le Goff *et al.* (2015), Korneva *et al.* (2016) and Jablonská *et al.* (2016; 2018) for the Apulian Platform margin (peri-Adriatic region); and Ortner (2007) for hemipelagic carbonates of the Eastern Alps.

Where found, the detailed analysis of gravity-driven structures and deposits developed in the slopes of carbonate platforms constitute a major contribution to the understanding of deep-marine processes. These have traditionally been better recorded in clastic systems thanks to seismic imaging carried out in petroleum exploration (see review by Bull *et al*., 2009). Such processes may control the internal architecture of the lower slopes of carbonate platforms (*e.g.* Kenter *et al.*, 2005); generate tsunamis (*e.g.* Løvholt *et al.*, 2018) or geohazards to offshore petroleum production (*e.g.* Bryn *et al.*, 2005); or influence fluid migration paths and the location of hydrocarbon reservoirs and traps (*e.g.* Hurst *et al.*, 2011; Kneller *et al.*, 2016). They are therefore features of considerable interest.

(Insert Fig. 1 here in full page)

3. Geological setting

The Cantabrian Zone conforms the foreland and thrust belt of the Variscan Orogen in the NW of the Iberian Massif (Figure 1A). It was deformed by thin-skinned tectonics, where several thrust units were emplaced during Pennsylvanian times (Julivert, 1971; Julivert, 1978). Earlier subdivisions of the Cantabrian Zone (Julivert, 1971; Pérez-Estaún *et al*., 1988) have recently been simplified by the recognition of the León Thrust, a major structure, as an out-of-sequence breaching thrust that duplicated some of the palaeogeographic domains (Alonso *et al.* 2009) (Figure 1A).

The study area (Figure 1B) is located in the southern sector of the Bodón-Ponga Unit (Alonso *et al.,* 2009). The emplacement of the thrust sheets of this and other units in the southern limb of the Cantabrian Variscan orocline was towards the NE, in direction to the foreland basin (Arboleya, 1981; Alonso, 1985; Alonso *et al.*, 1989). A late Variscan N-S shortening is recorded by the unconformable Stephanian succession, and caused fold tightening and thrust overturning in the southern branch of the Cantabrian Zone (Alonso *et al.*, 1987). During Late Carboniferous–Early Permian the initially linear orogen was affected by the Variscan oroclinal bending, responsible for the current arcuate structural trend of the Cantabrian Zone (Gutiérrez-Alonso *et al.*, 2004) (Figure 1A).

The rock record of the Cantabrian Zone is composed of a Proterozoic basement overlain by a Palaeozoic sedimentary cover deposited in the northern continental margin of Gondwana. The sedimentary basin evolved through three stages, namely rift, passive margin, and finally foreland basin. The latter transition, related to the onset of the Variscan orogeny, is either estimated to have taken place during the late Famenian (Keller, 2000; Keller *et al.,* 2007) or the earliest Mississippian (Colmenero *et al.*, 2002, and references therein).

During the foreland basin stage, a thick siliciclastic-dominated sequence was deposited. With the exception of the distalmost part of the basin, carbonate sedimentation took place mainly during the Early Carboniferous (Serpukhovian) and the Bashkirian. Serpukhovian extensive flat-lying, thin-bedded and laminated, dark grey mudstones (Barcaliente Formation) were succeeded by Bashkirian isolated carbonate platforms collectively referred to as the Valdeteja Formation (e.g. see Chesnel *et al.*, 2016). These platforms developed until the Late Bashkirian, when they were buried by the orogen-derived siliciclastics that build the majority of the overlying succession. In the distal margin, however, the onset of siliciclastic input was delayed allowing the initially isolated platforms to amalgamate into a single larger one, the Cuera/Picos de Europa platform, whose production finally ceased in the Early Kasimovian (Bahamonde et al., 2007, 2015; Merino-Tomé *et al.*, 2014).

The Variscan orogen was eroded away in Permian times, as evidenced by preserved isolated Permo- Mesozoic sediments that originally covered the Cantabrian Zone until the Alpine orogenic cycle, when as a western prolongation of the Pyrenees, a southward-verging blind crustal-scale thrust uplifted and exhumed the Variscan basement (Pulgar *et al.*, 1999; Gallastegui, 2000).

4. Methods

Fieldwork was conducted in order to build a general geological map of the area, with special emphasis on the detailed mapping of the more complex Pontedo Gorge area (Figure 1B). Mapping was performed on hardcopies of orthorectified aerial photographs from IGN (National Geographic Institute of Spain) with a resolution of 25 cm per pixel. Orthorectified images from Bing Maps server were used for mapping purposes as well. Structural data were acquired and a composite stratigraphic section of the studied succession was measured on localities around the gorge (Figure 2). The Pontedo Gorge map depicts the different sedimentary bodies and structures responsible for their deformation, and was built on a topographic map obtained from a digital elevation model supplied by the IGN (National Geographic Institute of Spain) with the aid of QGis® software. QGis® software was used to digitize the field map.

Structural measurements include orientation of fold limbs, axes, axial planes and axial traces, as well as fault planes, slickenlines, and associated cut-off lines. Axial surfaces were obtained by either (i) calculating the bisector plane of the fold limbs or (ii) calculating the plane that contain two lines, namely the fold axis and the axial trace. Both methods yielded similar results.

Structural data were graphically plotted in a lower hemisphere equal-area (Schmidt) stereographic projection for their statistical treatment and to restore the structures to their original position, with the aid of Stereonet software (Allmendinger *et al.*, 2012).

Due to the initial uncertainty with respect to the original slope orientation and dip, restoration was carried out to a horizontal position with the aim of obtaining the less conditioned results. The succession is overturned and shows different strike on both sides of the River Torío (Figure 2). Whereas in the western side the bedding dips on average 000/60, in the eastern side it changes to 037/51. This difference, related to late Variscan deformation, has been taken into account in the restoration: structures in the eastern side were initially restored to the current average orientation of stratification in the western side. All structures were subsequently restored carrying the bedding to a horizontal attitude, rotated about an axis that corresponds to the strike of the local stratification (commonly E–W) and an angle of rotation supplementary to the local dip (in the most common case of overturned strata).

After restoration diverse structures were analysed in order to estimate the transport sense on the basis of their vergence, estimated from fold axial planes and axes, as well as both normal and reverse faults, their associated slickenlines and cut-off lines.

Detailed geological profiles normal to fold axes were built with the aim of obtaining the actual geometry of structures, following the method described by Ragan (1968). Additionally, a general profile of the studied area was restored to the original configuration of the deposits, from which a shortening and thickening estimate has been obtained. Restoration has been accomplished through line-length balancing (*e.g.* Butler, 1987; Alsop *et al.*, 2017a for MTDs). The overturning of the thrusts in the southern branch of the Cantabrian Zone accounts for the fact that the map-view attitude of the structures provides a section oblique to the Variscan transport. In this fashion, the map view is apparently similar to the true (*i.e.* transport-parallel) geological profile (*e.g.* Alonso, 1987).

(Insert Fig. 2 here in full page)

5. Stratigraphy of the Pontedo Ravines

5.1 Overview

In the Pontedo Gorge a *ca.* 320m-thick deformed carbonate succession crops out, which belongs to the lower slope to basin-floor deposits of a carbonate platform of the Valdeteja Formation (Figure 3; Figure 2 for location). The massive boundstone limestones of the upper slope are intensely dolomitized in this area, thus hindering the recognition of their internal sedimentary features. Underlying the Valdeteja platform the laminated dark limestones of the Barcaliente Fm. display well-preserved 10–15cm-thick beds despite dolomitization.

The studied Valdeteja slope deposits mainly consist of undolomitized calcareous breccias and limestones, together with marlstones and shales. They have been divided into several sedimentary facies described in the following section.

(Insert Fig. 3 here)

5.2 Facies description and interpretation

5.2.1 Isolated blocks (V1)

Facies V1 consists of large blocks of light-grey-coloured microbial boundstone, identical to the upper-slope massive deposits of the Valdeteja platform. They range in size from a few meters to 325 m (Figure 4A), and appear as isolated bodies among breccia and calciturbidite beds that onlap their upper surfaces.

Based on their features and their stratal relation with the overlying layers, it has been interpreted that these blocks were detached from the upper slope and slid downslope towards the basin floor.

5.2.2 Matrix-rich boulder breccias (D)

Facies D1 constitutes chaotic deposits composed of meter-sized limestone boulders with variable textures (dark micrite, light-coloured boundstone, grainstone limestones, dismembered calciturbidite beds) embedded in a micrite matrix with floating sand-sized grains. Exceptionally, some boulders of microbial boundstones, similar to those of facies V1, reach decametric size. This facies forms decametre-thick lenticular massive units with an abrupt and non-erosive base and a lateral extent that ranges from tens to several hundreds of meters (Figure 4C). Most of these units crop out in the eastern river side, and stack vertically in a forestepping way suggesting an overall north-eastward progradation.

Facies D2 forms matrix-supported calcareous boulder breccias forming decimetre- to metre-thick beds that display non-erosive bases. Boulders are up to 30 cm in size, and as in the case of D1, display several limestone textures (Figure 4B).

Based on the non-erosive character of the basal contacts and the disorganized unsorted fabric of facies D1 and D2, it is interpreted that they were deposited from cohesive debris flows (debrites *sensu* Bouma, 1972; Nemec and Steel, 1984; Mutti, 1992).

5.2.3 Calclithites (C)

This facies consists of two facies, C1 and C2. Facies C1 are lithoclastic and bioclastic limestones that form 30–40-cm thick beds constitute facies C1. The clasts consist of slope- and platform-derived particles, including abundant crinoid ossicles. Beds display normal grading from pebble~~s~~ to medium sand. This facies commonly occurs interleaved with intercalations of spiculites (facies E1) and marlstones and shales (facies M1), in which case they usually contain chert nodules. This facies may occur filling small erosive depressions.

Facies C2 is similar to C1, but finer grained and more organized. It forms beds consisting of a lower graded division from fine gravel to fine sand, overlain by a second division of parallel laminated fine to very fine grained sand (Figure 4D), and finally capped by a division of shales and/or marlstones. Beds of this facies also interleave with spiculites (facies E1) and marlstones and shales (facies M1).

Based on their fabric and grain size, both facies have been interpreted as the result of different types of turbidity currents. Facies C1 is related to suspension–sedimentation and/or en-masse sedimentation from concentrated gravity flows (high-density turbidity currents; see Lowe, 1982). Conversely, facies C2 is interpreted as deposited from both high- and low-density turbidity currents (see Lowe, 1982).

5.2.4 Marlstones and thin bedded calclithites (M1)

Facies M1 consists of bedded and laminated marlstones/shales lithologically similar to those capping the beds of facies C2. It forms intervals up to few metres in thickness made of a stacking of marlstone and shale beds with a thin (up to a few cm-thick) basal division of very fine grained calcarenite/calclithite to calcisiltite.

M1 deposits are interpreted as the distal counterparts of facies C1 and C2, having been laid down from very dilute small-volume turbidity currents (Tc–e to Te beds after Bouma, 1962).

5.2.5 Spiculites (E1)

Facies E1 is composed of dark spiculite wackestone to fine-grained packstone limestones, often marly, with a variable content of calcitized sponge spicules, organized in cm-thick beds. Locally they contain bedding-parallel aligned chert nodules (Figure 4E).

Based on the locally preferred orientation of spicules, it is interpreted that they were transported by currents that carried them downslope, and deposited by dilute and small-volume flows similar to those of facies M1.

5.2.6 Sandstones (A1)

Facies A1 is made of sandstones forming tabular beds up to a few decimetres in thickness, with a sharp flat base, a normal grading from medium to very fine sand, and a gradational top into an overlying dark shale cap. This facies is exclusively found atop the carbonate sequence belonging to the overlying San Emiliano Formation.

This facies is interpreted as deposited from turbidity currents (Bouma, 1962; Lowe, 1982; Mutti, 1992; amongst others) carrying siliciclastic, orogen-derived sediments.

(Insert Fig. 4 here in full page)

5.3 Facies association and interpretation of the depositional setting

The mode of occurrence of the described facies permits to group them into a single facies association, defined by the coexistence of coarser (large slid blocks and debrites) and finer grained (turbidites) deposits. All of them resulted from gravity destabilization processes, leading to the generation of slid units (blocks), as well as to a wide range of other gravity-flow deposits. Both the facies and their association are consistent with those found in similar settings of other carbonate platforms in the Cantabrian Zone (Bahamonde *et al*., 1988; Bahamonde and Colmenero, 1993; Bahamonde *et al*., 1997; Della Porta *et al*. 2003; Bahamonde *et al.,* 2008; Chesnel *et al.*, 2016) and other regions (Masetti *et al.*, 1991; Kenter, 1990; among others).

Compared to these examples, and especially to the well preserved coeval platform described by Chesnel *et al.* (2016) in a neighbouring area, the facies association here described can be assigned to the transition from the lower slope to the proximal basin floor of one of the carbonate platforms of the Valdeteja Formation. This interpretation arises from the coexistence of relatively proximal (*i.e.* large slid blocks and debrites) and relatively distal (coarse and fine-grained turbidites) deposits and from the depositional slope compared to the palaeo-horizontal defined by the attitude of the underlying Barcaliente Fm. strata.

5.4 Paleocurrent

Paleocurrent indicators are scarce in the studied strata. Only two beds of facies C2 have groove casts exposed in their bases. Once restored to the horizontal position, they differ some 70°, indicating a SSW-NNE and WSW-ENE direction (Figure 4D). Despite being scarce, they are valuable objective data, whose reliability is backed by their mutual coincidence and their coherence with the regional and local data provided from mapping and palaeoslope reconstruction after bedding correction.

6. Sequential description of the slide and slump events in the area

In the following section the sequential development of the structures found in the study area is discussed.

(Insert Fig. 5 here)

6.1 Block sliding

The first event that took place in the toe of the slope was the sliding of several large blocks, ranging from 30 to 360 m in measured length. The blocks (facies V1) were detached from the upper slope, from which they slid towards the basin floor (Figure 5). A basal shear zone developed in the underlying deposits recorded the strain associated with the sliding process. It contains extensional faults that are interpreted as large-scale R-shears (Figures 5 and 6A&B).

After the sliding event, continued sedimentation buried the slide units with deposits of facies C1, C2, M1 and E1, which onlap the western and eastern margins of the main block (Figure 5). These deposits contain several debrite units of facies D1 and D2. Some of these deposits are affected by a vertically confined anticlinal–synclinal pair with dramatic hinge thickening (lower-right corner of Figure 5).

The transport sense obtained from the previous structures indicates a north-northeastward displacement in present coordinates (Figure 5).

Whether all the blocks in this sector originally formed part of a larger disintegrated single block or slid independently is uncertain. Farrell (1984) interpreted that blocking of the translation of the rear part of a hypothetical sliding block would result in a pulse of extensional stress in its still-moving frontal part, which could become detached from the rest of the body through listric faults converging into the main detachment surface along which sliding was taking place. That may be the origin of the smaller blocks, which are bounded at their rear end by extensional faults. The largest block is also crosscut by extensional faults and joints, but these did not lead to the separation of the resulting blocks.

(Insert Fig. 6 here)

6.2 Double thrust wedge

The second event caused the generation of a double thrust wedge that consists of two detachments and a backthrust ramp that transferred the displacement from the lower to the upper flat (Figure 7). This structure developed most likely as a consequence of the mechanical difficulties that arose as a result of the lower thrust sheet being emplaced below the large block. Under these circumstances, displacement was transferred upwards into a new thrust while the branch lines between the backthrust and lower and upper detachments continued their opposite propagation (see Martínez-Torres *et al.*, 1994) (Figure 7).

(Insert Fig. 7 here)

The extensional faults developed at the basal shear zone to the main block, now in the lower thrust sheet, were reactivated as backthrusts, some of which were generated during this event, also with associated folds. The reactivation is recorded by the preservation of a normal throw in the lower part and a reverse throw in the upper part of the succession (Figures 6A&B). A recumbent anticline was developed in the hangingwall ramp of the backthrust. Its overturned limb in the well-bedded basin deposits suggests that the large block, against which they onlap, was also folded during the backthrust movement (Figures 2 and 7).

In its eastern sector, the upper thrust crosscut two debrite units of facies D1 along a footwall ramp. The hangingwall ramp was accommodated to the thrust geometry through asymmetric folding, which generated an anticline–syncline pair developed ahead of the thrust tip line, interpreted as a fault-propagation fold. These folds locally display considerable hinge thickening of the finer deposits. Several minor thrusts imbricate from the main thrust, and display numerous minor structures, such as folds, extensional faults and backthrusts (Figures 6G and 8). Small-scale ramps display a strong parallelism in their cut-off lines and associated fold axes, both normal to slickensides.

The core of the main anticline is considerably complex, and shows a locally disharmonic folding style, with some axial planes converging into a single one. In this well-exposed core, a previous phase of shortening is recorded by bed-scale thrusting, backthrusting and stretching (extensional faults and local boudinage), with axes and cut-off lines slightly different (20° offset) to the main fold axial trends (Figures 6C-F and 9).

(Insert Fig. 8 here)

(Insert Fig. 9 here)

Refolded folds have been locally observed and measured. In one example, at least three folding phases have been identified (Figures 6H and 10). The earliest event consisted on the propagation of bed-scale thrusts with associated hangingwall and footwall folds. The second event consisted on the folding of the multilayer: the axial plane dips towards the NE, and hence it is interpreted to be associated with a backthrust. The axes of this event display a considerable dispersion in their orientation. The third event folded the previous fold. Both folds share a common axis orientation, and thus can be classified as type 3 folding interference (Ramsay, 1967).

(Insert Fig. 10 here)

When well-exposed, the deposits show coexistence of small-scale contractional and extensional structures, including folds, thrusts, backthrusts and extensional faults, all of them indicating a common transport direction. Orthogonal sets of extension fractures, with one of the sets with the strike normal to the transport direction, are also commonly found. Fold hinges also display orthogonal or slightly oblique extension sets, in numerous cases in the internal arc, where shortening rather than extension is commonly expected, in which case at least one of the sets has a strike parallel to the fold axis, suggesting a common origin. Some of the most competent C1 and C2 beds are sometimes boudinaged, with their necks parallel to the fold axes. This coexistence records concomitant transport-parallel shortening and extension.

Transport direction and sense has been determined from the orientation of all the previously mentioned structures, including the reactivated extensional faults in the basal shear zone, the backthrust-related anticline, the hangingwall folds associated to the upper thrust, and the bed-scale contractional and extensional structures. The estimated transport sense is towards the northeast in present coordinates (Figure 7).

6.3 Folding and steepening of the backthrust

Subsequently to the development of the double wedge, a new thrust was nucleated below the backthrust ramp (Figure 11). This thrust, which accommodates very little displacement, developed an anticline on the hangingwall ramp and a small syncline in the footwall. Furthermore, the sequence was translated some meters along the basal thrust of the double wedge, causing the folding of the deposits that onlap its frontal sector (Figure 11).

A northeastward transport sense for this event has been deduced from the orientation of the aforementioned structures (Figure 11).

(Insert Fig. 11 here)

(Insert Fig. 12 here in full page)

7. Discussion

7.1 Structural evolution through section restoration

The previously mentioned sequence of events has been deduced from the restoration of a geological profile constructed normal to the average fold axes (Figure 12). The restoration has not taken into account the strain accommodated by the marlstone-rich succession. Therefore, the estimated shortening is a minimum estimation, considering the fact that accommodation of deformation through internal strain may have been relatively large. Flow of material out of the profile section is suggested by the existence of sets of extensional fractures parallel to the transport direction (see sections 7.3.1 and 7.3.2), which also adds a degree of uncertainty in the accuracy of the shortening estimates interpreted from line-length balancing. The sequence in this sector was shortened in 205 m, which represents a relative 9.9% shortening.

7.2 Transport direction

Deformation in most of the Cantabrian Zone took place below metamorphic conditions (Brime, 1991), and is characterized by the development of frontal, oblique and lateral thrust ramps with associated folds (Pérez-Estaún *et al.*, 1988). The emplacement of the thrust units located in the southern limb of the Cantabrian orocline was northeastwards in present coordinates, as obtained from a variety of kinematic markers, including thrust cut-off and branch lines, fold orientations and basal-shear-zone mesostructures (Arboleya, 1981; Alonso, 1987; Alonso *et al.*, 1989).

The structures that affected the succession in the Pontedo Gorge display a relative scatter in their orientation. These indicate transport senses that vary from northward to eastward in present coordinates, with an average azimuth directed at N 32° E. The variable orientation of thrust surfaces and cut-off lines is attributed to their ramp orientation, which may vary from purely frontal to oblique or even lateral (Figure 13A&B). The parallelism in the orientation of thrust cut-off lines and associated fold axes, and their orthogonal relation with the locally measured slickenlines suggests that the largest thrusts are frontal structures (Figures 7-11). The scatter of extensional features, and most notably, of fold axes, is discussed in the following section (Figure 13).

The similar structures (thrusts and associated folds) resulting from the Variscan deformation and those observed in the Pontedo Gorge, and their common transport sense towards the NE, argue for the need of establishing a series of characteristics that allow the distinction between tectonic and gravity-driven deformation features.

7.3 Distinguishing gravitational from tectonic deformation

The following structural features are consistent with soft-sediment deformation caused by gravity-driven processes in the Pontedo section.

7.3.1 Deformation of poorly lithified sediments

Soft-sediment deformation triggered by the destabilization and collapse of thrust fronts and platform margins has been described in the Cantabrian Zone (Maas and Van Ginkel, 1983; Alonso *et al.*, 2006; Alonso *et al*., 2015). The geological context of the Valdeteja Fm. within the basin favours the gravitational origin for soft-sediment deformation caused by carbonate-platform-margin collapse. The array of Valdeteja carbonate platforms grew in the foreland basin of the Variscan Orogen during the Early to Late Bashkirian (*ca.* 322-317 Ma, Chesnel *et al.*, 2016), with an intervening foredeep with terrigenous turbidite sedimentation of the San Emiliano Fm. (*ca.* 316-312 Ma, Chesnel *et al.,* 2016) (*e.g.* Colmenero *et al*., 2002; Merino-Tomé *et al.*, 2014; Chesnel *et al*., 2016). Ensuing sedimentation during the evolution of the foreland basin resulted in the burial of the Valdeteja platforms under a mainly siliciclastic sedimentary pile, whose thickness is difficult to estimate due to further erosion but that reached 6000 m in some places and exceeded 1500–2000 m in the study area (cf. Colmenero *et al*., 2002 and references therein). Emplacement of the Bodón-Ponga Unit started during the Late Moscovian–Early Kasimovian (*ca.* 307 Ma, Alonso *et al*., 2006), and therefore, *ca.* 10 Myr elapsed between sedimentation of the Valdeteja Fm. slope deposits and the onset of Variscan deformation in the Pontedo area. Comparison with data from Miocene (some 10–13 Myr old) deep-water deposits, buried at depths greater than 550–700 mbsf and ranging in composition from clay-rich and carbonate-poor (cf. Shipboard Scientific Party, 2000a,b) to carbonate-rich with shallow-water grains (cf. Turpin *et al*., 2008) permits to interpret that by the time tectonic deformation cannibalized the Valdeteja platforms, the sediments were well lithified. This assumption is backed by the structural style displayed elsewhere in the Cantabrian Zone foreland basin not only by the same or other stratigraphic intervals of the same age and/or depth of burial but also by younger and/or shallower units. Nevertheless, despite these facts several lines of evidence indicate that deformation in the Pontedo area took place in poorly lithified sediments.

Firstly, hinge thickening is observed where thick marlstone and shale packages are folded. Flow of incompetent material into the fold hinges may cause a 1600% increase in thickness in the most extreme case (Figure 5). Therefore, the mechanically weakest lithologies (marlstones, shales and spiculites in the studied examples) are those that display class III fold geometries of Ramsay (1967). According to Waldron and Gagnon (2011), this would indicate that fluids had already escaped from the granular, sand- and gravel-grade lithologies ("sandy" lithologies in these authors' nomenclature). This is supported by the coherent behaviour of the beds involved in the deformation, which have preserved their sedimentary structure (Corbett, 1973; Alsop and Marco, 2013). The bedded deposits may have preserved their internal consistency due to the low pore pressure existing during deformation, which hampered the loss of internal shear resistance and hindered their liquefaction (Knipe, 1986; Owen, 1996; Spalluto *et al.*, 2007; Le Goff *et al.*, 2015). Hinge-thickening is one of the most accepted indicators of deformation of poorly-lithified sediments (Ortner, 2007; Waldron and Gagnon, 2011; Jablonská *et al.*, 2018). Nevertheless, it must be treated with caution, as hinge thickening is a rather common feature observed in the Cantabrian Zone and elsewhere (Ramsay, 1974) in layered sequences that exhibit rheologically-contrasting lithologies. Notwithstanding this fact, the dramatic thickening observed in the sequence of the Pontedo Gorge is unparalleled elsewhere in the Cantabrian Zone.

Secondly, surfaces resembling hydroplastic fractures, known to develop during soft-sediment deformation (Petit and Laville, 1987), are a common feature in the lower-slope and basin-floor deposits of the Pontedo Gorge, both in flat beds and in fold hinges (Figure 6E&F). At least one of their sets is often normal to the transport direction. The existence of several sets, with generally two of them normal to each other, indicates a clear departure from plane strain conditions, and has been observed in other gravity-driven deposits in the Cantabrian Zone (Alonso *et al.*, 2006) and elsewhere (Alsop and Marco, 2011).

In third place, the sequence displays examples of refolded folds (Figure 6H and 10). These type of outcrop-scale deformation is nowhere to be seen in the Cantabrian Zone related to the Variscan deformation. On the other hand, refolding of folds is a relatively common observation within gravity-deformed thrust and slump sheets affecting poorly lithified sediments (*e.g.* Ortner, 2007; Alsop and Marco, 2013).

Finally, bed-scale thrust ramps are welded, suggesting that diagenesis took place after this deformation.

7.3.2 Scatter of kinematic indicators

The scatter displayed in the orientation of extensional faults and joints is attributed to the existence of a component of non-plane strain that locally induced transport-oblique to transport-normal extension (Figure 13C&D). This has been observed in other examples of soft-sediment slump-related deformation, in which significant out-of-plane material movement may take place (Alonso *et al.*, 2006; Alsop and Marco, 2011).

The scatter in fold axes orientations (up to 90°, Figure 13E&F) is an acknowledged characteristic of gravity-driven deformation (Strachan and Alsop, 2006; Ortner, 2007; Jablonská *et al.*, 2018). It may be caused by (i) variations in the shear strain imposed on the slumped succession, which influences fold tightening and axes orientations (Strachan and Alsop, 2006; Ortner, 2007; Alsop and Marco, 2011, Jablonská *et al.*, 2018); (ii) variations in escarpment surfaces orientation (Jablonská et al., 2016), or (iii) variations in the orientation of the thrust ramps, from purely frontal to slightly oblique. Nevertheless, and despite their scatter in the Pontedo Gorge, fold axes still cluster around a N 130° E trend, an observation consistent with the coherent style of deformation. Folds in coherently deformed areas are mostly subjected to layer-parallel shear, with only limited lateral shear strain variations, and they tend to preserve axial trends at high angles to the slope dip direction (Alsop and Marco, 2013).

Overall, all deformation structures record a north-eastwards transport sense that coincides with the SSW-NNE and WSW-ENE paleocurrent orientations determined from scarce groove casts of calciturbidite beds (Figure 4D). While this is not evidence for the gravity-driven generation of structures in itself, it is consistent with the interpretation.

(Insert Fig. 13 here in full page)

7.3.3 Unrooted deformation

Thrusts are restricted to the slope deposits. Mapping precludes their rooting in a regional-scale structure that cuts downwards into the stratigraphic succession. Basal detachments are thus rootless, and they are better interpreted as the basal detachment surfaces of gravitational collapse slump structures related to the carbonate-platform slope ("superficial deformation" of Waldron and Gagnon, 2011). Towards the west, two low-angle normal faults that crosscut the lower slope sequence converge into a basal detachment which can be followed into the basal thrust that affects the sequence in the Pontedo Gorge section (Figure 14A). Rollover folds associated to these faults indicate extension towards the north, an orientation consistent with the range of transport directions derived from contractional structures in the Pontedo Gorge. Therefore, these faults are interpreted as associated to slope failure, whose extension led to shortening at the toe of the slope.

Mapping of the Pontedo Gorge and neighbouring areas also shows that the described structures affecting the Valdeteja Fm. deposits cannot be traced upwards into younger stratigraphic levels, in such way that the first limestone unit of the overlying San Emiliano Formation, the so-called "caliza masiva" (Moore *et al*., 1971), is not involved in the deformation (Figure 1B).

Towards the east from the Pontedo section, the contact between the carbonate platform and slope deposits shows several inflection points that bound sectors with a concave-up listric geometry, where evidence of extensional faults has been observed, including fault slickensides and slickenlines, cut-off lines, drag synclines, rollover anticlines or the onlap of lower-slope–basin strata. The restored strike of some measured faults and scar slumps is NW-SE, with their slickenlines indicating a transport direction towards the NE, in agreement with the smaller-scale structures found in the Pontedo Gorge (Figure 14B). Other conjugated faults display a restored SW-NE trend, indicating a component of non-plane strain, that is, of extension normal to the transport direction, similar to the observed at the small-scale in Pontedo. Rollover folds associated to the faults display their axes W-E, though their scarcity precludes a kinematic interpretation (Figure 14B). These listric surfaces affect progressively younger sequence intervals towards the east, and their geometry and stratigraphic relationships permit to interpret them as extensional faults and large slump scars that succeeded one another in time and that were finally buried by San Emiliano strata.

(Insert Fig. 14 here)

7.3.4 Coexistence of contractional and extensional features

Contractional and extensional structures are often found together and without reactivation, suggesting that were originated at the same time. This supposition is reinforced by the perfect match in the transport direction independently assessed by analysing their orientation: fold hinges and bed-scale thrust cut-off lines are parallel to bed-scale extensional faults and joints cut-offs and boudin necks affecting the more competent strata (Figure 13). Such a coexistence of structures is to be expected in a translating sediment mass, where slight differences in velocity within the slumped unit may generate areas that undergo extension (fast or accelerating velocity) and areas that undergo shortening (slow or decelerating velocity) (Farrell, 1984). These spatial variations in velocity constitute a “flow cell”, and several of them may be present within a slumped unit varying their position through time (Alsop and Marco, 2014). As a result of this multi-cell flow model, extensional features may overprint previous contractional structures, and vice versa, during a single slump event, and as a result they will share a common trend (Alsop and Marco, 2014).

7.3.5 Relation of the structures with the depositional setting

As argued, the sediments involved in the deformation were deposited in the transition from the lower slope to the proximal basin floor of one of the carbonate platforms of the Valdeteja Formation. The sedimentary succession itself is the result of mass wasting processes of different types, including block sliding (facies V1), debris flows (facies D1&2) and turbidity currents (facies C1&2). Furthermore, because of the change in slope, the toe of the slope is an ideal location for the displacement caused by extensional failures in the slope being transferred into contractional structures. Although the location itself is not evidence for gravitationally-induced deformation, it is consistent with the interpretation.

On the basis of the previous arguments, it is interpreted that the contractional and extensional structures found in the Pontedo Gorge were induced by gravitational instabilities within the slope of a Valdeteja carbonate platform. In the basis of the estimated transport directions, the strike of the slope was roughly WNW-ESE, and its dip towards the NE, that is to say, away from the foredeep of the foreland basin.

8. Conclusions

The platform top and the upper slope of an isolated carbonate platform of the Valdeteja Fm. in the Bodón–Ponga Unit of the Cantabrian Zone (Pontedo Gorge section) underwent gravitational collapse that resulted in the transfer of sedimentary masses towards the lower-slope–basin floor, where they accumulated as slide blocks, debrites and turbidites, which ultimately underwent slumping processes. The slump units progressively deformed during their transport, which took place while they were still partially lithified. This interpretation is supported by features such as soft-sediment deformation, transport sense and scatter of kinematic indicators, paleocurrent orientations, unrooted deformation, coexistence of contractional and extensional structures, and the relation of the structures with the depositional setting.

A detailed analysis of the deformation structures and their restoration to an initially horizontal position has allowed the identification of transport directions towards the north-northeast and northeast. This result indicates that the carbonate platform displayed an approximately WNW-ESE trending margin and NE-dipping slope, facing the foreland, and provides new constraints on the orientation and characteristics of the isolated carbonate platforms of the Valdeteja Formation developed in the foreland basin of the Cantabrian Zone during the Bashkirian.

9. Acknowledgements

This work was supported by the Ministry of Economy and Competitiveness of Spain (MINECO) through the research project CGL2012-34475. Óscar Merino-Tomé is thanked for his helpful comments in the field. We would also like to thank the editor Ian Alsop and two anonymous referees for their constructive reviews and recommendations.

10. References

Allmendinger, R.W., Cardozo, N., Fisher, D., 2012. Structural geology algorithms: Vectors and tensors in structural geology. Cambridge University Press.

Alonso, J.L., 1987. Sequences of thrusts and displacement transfer in the superposed duplexes of the Esla Nappe Region (Cantabrian Zone, NW Spain). Journal of Structural Geology, 9 (8), 969-983.

Alonso, J.L., Álvarez Marrón J., Pulgar, J.A., 1989. Síntesis cartográfica de la parte sudoccidental de la Zona Cantábrica. Trabajos de Geología 18, 145-153.

Alonso, J.L., Marcos, A., Suárez, A., 2006. Structure and organization of the Porma mélange: Progressive denudation of a submarine nappe toe by gravitational collapse. American Journal of Science 306, 32-65.

Alonso, J.L., Marcos, A., Suárez, A., 2009. Paleogeographic inversion resulting from large out of sequence breaching thrusts: The León Fault (Cantabrian Zone, NW Iberia). A new picture of the external Variscan Thrust Belt in the Ibero-Armorican Arc. Geologica Acta 7, 451-473.

Alonso, J.L., Marcos, A., Villa, E., Suárez, A., Merino-Tomé, O., Fernández, L.P., 2015. Mélanges and other types of block-in-matrix formations in the Cantabrian Zone (Variscan Orogen, northwest Spain): origin and significance. International Geology Review 57, 563-580.

Arboleya, M.L. (1981). La estructura del Manto del Esla (Cordillera Cantábrica, León). Boletín Geológico y Minero, 42, 1, 19-40.

Alsop, G.I., Marco, S., 2011. Soft-sediment deformation within seismogenic slumps of the Dead Sea Basin. Journal of Structural Geology 33, 433-457.

Alsop, G. I., Marco, S., 2013. Seismogenic slump folds formed by gravity-driven tectonics down a negligible subaqueous slope. Tectonophysics, 605, 48-69.

Alsop, G.I., Marco, S., 2014. Fold and fabric relationships in temporally and spatially evolving slump systems: A multi-cell flow model. Journal of Structural Geology, 63, 27-49.

Alsop, G.I., Marco, S., Levi, T., Weinberger, R., 2017a. Fold and thrust systems in Mass Transport Deposits. Journal of Structural Geology, 94, 98-115.

Alsop, G.I., Weinberger, R., Marco, S., Levi, T., 2017b. Identifying soft-sediment deformation in rocks. Journal of Structural Geology, doi.org/10.1016/j.jsg.2017.09.001.

Alsop, G.I., Weinberger, R., Marco, S., 2018. Distinguishing thrust sequences in gravity-driven fold and thrust belts. Journal of Structural Geology, 109, 99-119.

Bahamonde, J.R., Colmenero, J.R., Heredia, N., 1988. Morfología de un margen de plataforma carbonatada en el Carbonífero Superior de la Zona Cantábrica. Geogaceta 5, 48-50.

Bahamonde, J.R. y Colmenero, J.R., 1993. Análisis estratigráfico del Carbonífero Medio y Superior del Manto del Ponga (Zona Cantábrica). Trabajos de Geología 19, 155-193.

Bahamonde, J.R., Merino-Tomé, O., Heredia, N., 2007. Pennsylvanian microbial boundstone-dominated carbonate shelf developed in a distal foreland margin (Picos de Europa Province, NW Spain). Sedimentary Geology, 198, 167–193.

Bahamonde, J.R., Vera, C., Colmenero, J.R., 1997. Geometría y facies del margen progradante de una plataforma carbonatada (Unidad de Picos de Europa, Zona Cantábrica). Revista de la Sociedad Geológica de España 10, 1-2, 163-181.

Bahamonde, J.R., Kenter, J.A.M., Della Porta, G., van Hoeflaken, F., 2008. Facies belts of a Carboniferous carbonate platform (San Antolín-La Huelga section, NE Cantabrian Zone, Northern Spain). Trabajos de Geología 28, 69-86.

Bahamonde, J.R., Merino-Tomé, O., Della Porta, G., Villa, E., 2015, Pennsylvanian carbonate platforms adjacent to deltaic systems in an active marine foreland basin (Escalada Fm., Cantabrian Zone, NW Spain). Basin Research, 27, 208–229,

Bouma, A.H., 1962. Sedimentology of some Flysch deposits: A graphic approach to facies interpretation. Elsevier, Amsterdam.

Bouma, A.H., 1972. Recent and ancient turbidites and contourites. Gulf Coast Association of Geological Societies Transactions, 22, 205-221.

Brime, C., 1991. Metamorphism in the northeastern Iberian Massif (NW Spain). In: Browne, P.L. and Simmons, S.F. (Eds.): Low temperature metamorphic processes in contrasting geodynamic settings. Auckland, New Zealand, 10.

Bull, S., Cartwright, J., Huuse, M., 2009. A review of kinematic indicators from mass-transport complexes using 3D seismic data. Marine and Petroleum Geology 26, 1132-1151.

Bryn, P., Berg, K., Forsberg, C.F., Solheim, A., Kvalstad, T.J., 2005. Explaining the Storegga Slide. Marine and Petroleum Geology, 22, 11-19.

Butler, R.W.H, 1987. Thrust sequences. Journal of the Geological Society of London, 144 (4), 619-634.

Chesnel, V., Samankassou, E., Merino-Tomé, O., Fernández, L.P., Villa, E., 2016. Facies, geometry and growth phases of the Valdorria carbonate platform (Pennsylvanian, northern Spain). Sedimentology 63, 60-104.

Colmenero, J.R., Fernández, L.P., Moreno, C., Bahamonde, J.R., Barba, P., Heredia, N., González, F., 2002. Carboniferous. In: Gibbons, W., Moreno, T. (Eds.), The Geology of Spain. Geological Society, London, 116.

Corbett, K. D., 1973. Open-cast slump sheets and their relationship to sandstone beds in an Upper Cambrian flysch sequence, Tasmania. Journal of Sedimentary Petrology, 43 (1), 147-159.

Elliot, C.G., Williams, P.F., 1988. Sediment slump structures: a review of diagnostic criteria and application to an example from Newfoundland. Journal of Structural Geology 10, 171-182.

Dasgupta, P., 2008. Experimental decipherment of the soft-sediment deformation observed in the upper part of the Talchir Formation (Lower Permian), Jharia Basin, India. Sedimentary Geology, 205, 100-110.

Della Porta, G., Kenter, J.A.M., Bahamonde, J.R., Immenhauser, A., Villa, E., 2003. Microbial boundstone dominated carbonate slope (Upper Carboniferous, N Spain): microfacies, lithofacies distribution and stratal geometry. Facies 49, 175-208.

Elliott, C. G., Williams, P. F., 1988. Sediment slump structures: a review of diagnostic criteria and application to an example from Newfoundland. Journal of Structural Geology, 10 (2), 171-182.

Farrell, S.G., 1984. A dislocation model applied to slump structures, Ainsa Basin, South Central Pyrenees. Journal of Structural Geology 6, 727-736.

Gallastegui, J., 2000. Estructura cortical de la cordillera y margen continental cantábricos: perfiles ESCI-N. Trabajos de Geología 22, 9-234.

Gutiérrez-Alonso, G., Fernández-Suárez, J., Weil, A.B., 2004. Orocline triggered lithospheric delamination. In: Sussman, A.J. and Weil, A.B. (Eds.), Orogenic Curvature: Integrating Paleomagnetic and Structural Analyses. GSA Special Paper 383, 121-130.

Hanson, E., 1971. Strain Facies. Springer-Verlag, New York.

Helwig, J., 1970. Slump folds and early structures, Northeastern Newfoundland Appalachians. The Journal of Geology 78, 172-187.

Hurst, A., Scott, A., Vigorito, M., 2011. Physical characteristics of sand injectites. Earth-Science Reviews, 106 (3-4), 215-246.

Jablonská, D., Di Celma, C., Korneva, I., Tondi, E., Alsop, I. (2016). Mass-transport deposits within basinal carbonates from southern Italy. Italian Journal of Geosciences1 135, 1, 30-40.

Jablonská, D., di Celma, C.N., Alsop, G.I., Tondi, E., 2018. Internal architecture of mass-transport deposits in basinal carbonates: a case study from southern Italy. Sedimentology, 65, 1246-1276.

Julivert, M., 1971. Décollement tectonics in the Hercynian cordillera of NW Spain. American Journal of Science 270, 1-29.

Julivert, M., 1978. Hercynian orogeny and carboniferous paleogeography in NW Spain: a model of deformation-sedimentation relationships. Zeitschrift der Deutschen Geologischen Gesellschaft, 129, 565-592.

Keller, M., 2000. La cuenca de antepaís Cantábrica, ¿un fenómeno Devónico o Carbonífero? Geotemas 1, 285-288.

Keller, M., Bahlburg, H., Reuther, C.D., Weh, A., 2007. Flexural to broken foreland basin evolution as a result of Variscan collisional events in northwestern Spain. In: Hatcher, R.D., Jr, Carlson, M.P., McBride, J.H., Martínez-Catalán, J.R. (Eds.), 4-D Framework of Continental Crust: Geological Society of America Memoir 200, 489-510.

Kenter, J.A.M., 1990. Carbonate platform flanks: slope angle and sediment fabric. Sedimentology 37, 777-794.

Kenter, J.A.M., Harris, P.M., Della Porta, G., 2005. Steep microbial boundstone-dominated platform margins – Examples and implications. Sedimentary Geology, 178, 5–30.

Kneller, B., Dykstra, M., Fairweather, K., Milana, J.P., 2016. Mass-transport and slope accommodation: Implications for turbidite sandstone reservoirs. AAPG Bulletin, 100, 213-235.

Knipe, R.J., 1986. Deformation mechanism path diagrams for sediments undergoing lithification. Memoir of the Geological Society of America 166, 151–160.

Korneva, I., Tondi, E., Jablonská, D., Di Celma, C., Alsop, I., Agosta, F. (2016). Distinguishing tectonically- and gravity-driven synsedimentary deformation structures along the Apulian platform margin (Gargano Promontory, southern Italy). Marine and Petroleum Geology, 73, 479-491.

Le Goff, J., Cerepi, A., Swennen, R., Loisy, C., Caron, M., Muska, K., El Desouky, H., 2015. Contribution to the understanding of the Ionian Basin sedimentary evolution along the eastern edge of Apulia during the Late Cretaceous in Albania. Sedimentary Geology, 317, 87-101.

Løvholt, F., Schulten, I., Mosher, D., Harbitz, C., Krastel, S., 2018. Modelling the 1929 Grand Banks slump and landslide tsunami. In: Lintern, D.G., Mosher, D.C., *et al.* (Eds.). Subaqueous Mass Movements and their Consequences, Geological Society, London, Special Publications, 477, https://doi.org/10.1144/SP477.28.

Lowe, D.R., 1982. Sediment gravity flows: II. Depositional models with special reference to the deposits of high-density turbidity currents. Journal of Sedimentary Petrology 52, 279-297.

Maas, K., Van Ginkel, A.C., 1983. Variscan olistostrome deposition and synsedimentary nappe emplacement, Valdeón Area, Cantabrian Mountains, Spain. Leidse Geologische Mededelingen 52, 2, 341-381.

Maltman, A., 1984. On the term 'soft-sediment deformation'. Journal of Structural Geology 6, 589-592.

Martínez-Torres, L.M., Ramón-Lluch, R., Eguiluz, L., 1994. Tectonic wedges: geometry and kinematic interpretation. Journal of Structural Geology, 16 (10), 1491-1494.

Masetti, D., Neri, C., Bosellini, A., 1991. Deep-water asymmetric cycles and progradation of carbonate platforms governed by high-frequency eustatic oscillations (Triassic of the Dolomites, Italy). Geology 19, 336-339.

Merino-Tomé, O., Bahamonde, J.R., Della Porta, G., Chesnel, V., Villa, E., Samankassou, E., Fernández, L.P., 2014. The palaeoequatorial microbial carbonate province of the Cantabrian Zone (Pennsylvanian, NW Spain). Conference Paper of the 19th International Sedimentological Conference, Geneva, Switzerland.

Moore, L.R., Neves, R., Wagner, R.H., Wagner-Gentis, C.H.T., 1971. The stratigraphy of Namurian and Westphalian rocks in the Villamanín area of Northern León, N.W. Spain. Trabajos de Geología, 3, 307-363.

Mutti, E., 1992. Turbidite sandstones. Agip, Istituto di geologia, Università di Parma.

Nemec, W., Steel, R.J., 1984. Alluvial and coastal conglomerates: Their significant features and some comments on gravelly mass flow deposits. In: Koster, E.H., Steel, R.J. (Eds.), Sedimentology of gravels and conglomerates. Canadian Society of Petroleum Geologists Memoir, 10, 1-31.

Ortner, H., 2007. Styles of soft-sediment deformation on top of a growing fold system in the Gosau Group at Muttekopf, Northern Calcareous Alps, Austria: Slumping versus tectonic deformation. Sedimentary Geology, 196, 99-118.

Owen, G., 1996. Experimental soft-sediment deformation: structures formed by the liquefaction of unconsolidated sands and some ancient examples. Sedimentology, 43, 279-293.

Pérez-Estaún, A., Bastida, F., Alonso, J.L., Marquínez, J., Aller, J., Álvarez-Marrón, J., Marcos, A., Pulgar, J.A., 1988. A thin-skinned tectonic model for an arcuate fold and thrust belt: Cantabrian Zone (Variscan Ibero-Armorican Arc). Tectonics 7, 3, 517-537.

Petit, J.P., and Laville, E., 1987. Morphology and microstructures of hydroplastic slickensides in sandstone. In: Jones, M.E., Preston, R.M.F. (Eds.), Deformation of Sediments and Sedimentary Rocks. Geological Society of London Special Publication 29, 107-121.

Pulgar, J.A., Alonso, J.L., Espina, R.G., Marín, J.A., 1999. La deformación alpina en el basamento varisco de la Zona Cantábrica. Trabajos de Geología 21, 283-294.

Ragan, D.M., 1968. Structural geology: an introduction to geometrical techniques. John Wiley & Sons, New York.

Ramsay, J.G., 1967. Folding and Fracturing of Rocks. McGraw Hill, San Francisco.

Ramsay, J. G., 1974. Development of chevron folds. Geological Society of America Bulletin, 85 (11), 1741-1754.Shanmugam, G., Lehtonen, L.R., Straume, T., Syversten, S.E., Hodgkinson, R.J., Skibeli, M., 1994. Slump and debris flow dominated upper slope facies in the Cretaceous of the Norwegian North Seas (61-67 N): implications for sand distribution. AAPG Bulletin, 78, 910-937.

Shipboard Scientific Party, 2000. Site 1150. In: Sacks, I.S., Suyehiro, K., Acton, G.D., et al., Proc. ODP, Init. Repts., 186, 1–209 [CD-ROM]. Available from: Ocean Drilling Program, Texas A&M University, College Station TX 77845-9547, USA.

Shipboard Scientific Party, 2000. Site 1151. In: Sacks, I.S., Suyehiro, K., Acton, G.D., et al., Proc. ODP, Init. Repts., 186, 1–131 [CD-ROM]. Available from: Ocean Drilling Program, Texas A&M University, College Station TX 77845-9547, USA.

Spalluto, L., Moretti, M., Festa, V., Tropeano, M., 2007. Seismically-induced slumps in Lower-Maastrichtian peritidal carbonates of the Apulian Platform (southern Italy). Sedimentary Geology, 196, 81-98.

Stow, D.A.V., 1985. Deep-sea clastics: where are we and where are we going? In: Brenchly, P.J., Williams, P.J. (Eds.), Sedimentology: Recent Developments and Applied Aspects. Geological Society, London, Special Publication, Blackwell Scientific Publications, Oxford. 67-94.

Stow, D.A.V., 1994. Deep-sea processes of sediment transport and deposition. In: Pye, K. (Ed.), Sediment Transport and Depositional Processes. Blackwell, London, 257-291.

Stow, D.A.V., Reading, H.G., Collinson, J.D., 1996. Deep seas. In: Reading, H.G. (Ed.), Sedimentary Environments. Blackwell, London, 395-453.

Strachan, L.J., Alsop, G.I., 2006. Slump folds as estimators of palaeoslope: a case study from the Fisherstreet Slump of County Clare, Ireland. Basin Research 18, 451-470.

Turpin, M., Emmanuel, L., Renard, M., 2008. Nature and origin of carbonate particles along a transect on the western margin of Great Bahama Bank during the Middle Miocene: sedimentary processes and depositional model. Bulletin de la Societé Géologique de France, 179(3):231–244.

van der Merwe, W.C., Hodgson, D.M., Flint, S.S., 2011. Origin and terminal architecture of a submarine slide: a case study from the Permian Vischkuil Formation, Karoo Basin, South Africa. Sedimentology, 58, 2012-2038.

Waldron, J.W.F., Gagnon, J.F., 2011. Recognizing soft-sediment structures in deformed rocks of orogens. Journal of Structural Geology 33, 271-279.

Woodcock, N.H., 1979. The use of slump structures as palaeoslope orientation estimators. Sedimentology 26, 83-99.

Figure captions

FIGURE 1. (A) Geological map of the Cantabrian Zone showing its recent-most subdivision (modified from Alonso *et al.*, 2009). (B) General map of the northernmost sector of the Bodón Nappe. Boxed area indicates the location of the Pontedo Gorge area, where a detailed map has been elaborated (Fig. 2).

FIGURE 2. Detailed geological map of the Pontedo Gorge area.

FIGURE 3. Detailed stratigraphic log of the studied interval of the Valdeteja Fm. Duplicated interval is shadowed.

FIGURE 4. Field photographs of the sedimentary facies. Arrows indicate the top of the succession (notice it is overturned in all cases). (A) Large block (325 m) of facies V1 eroded by the Torío River. (B) Detail of facies D2. (C) Fieldwork aspect of facies D1 (cliff is *ca.* 12 m-high). (D) Facies C2 bed composed of a graded division, overlain by a laminated division and a final mudstone cap. Restored orientations of groove casts developed parallel to the paleocurrent are indicated. (E) Facies E1. Notice the nodular appearance of some beds.

FIGURE 5. Restored profile of the first deformation event. Lower-hemisphere equal-area stereoplots of the restored structures are referred to their location with a thin black arrow. Legend indicates the structural elements in the stereoplots. Orientation is referred to the restored section. Stratigraphic top is towards top of page.

FIGURE 6. Field photographs of structural features. Arrows indicate the top of the succession. (A) Basal shear zone below the large block of facies V1, developed in facies C1 and E1. Note that the succession is overturned. (B) Interpretation of A, with red thrusts and a reactivated extensional fault (note the change in throw along the easternmost fault, normal in the lower part and reverse in the upper part). (C) Bed-scale compressional structures in facies C2 (location 3 m to the south-east from E). (D) Interpretation of C:

note the development of a small-scale double thrust wedge. (E) Bed-scale extensional structures in facies C2 (see boudin necks in Figure 9 for location). (F) Interpretation of E: note the boudinage in the lower bed, and the orthogonal relation between two sets of hydroplastic fractures. The trends of red and green sets are, respectively, normal and parallel to transport sense. (G) Bed-scale view of imbricate thrusts (see Figure 8B for interpretation). (H) Refolded fold seen in lateral view in a road cut (see Figure 10 for interpretation).

FIGURE 7. Restored profile of the second deformation event and lower-hemisphere equal-area stereoplots of the restored structures. Location of figures 8 and 9 (subparallel sections to the profile) and 10 (lateral view, at high angle to the profile) is indicated. Orientation is referred to the restored section. Stratigraphic top is towards top of page.

FIGURE 8. Detailed map (A) and interpreted photograph (B, see Figure 6G) of locations in the imbricate thrusts branched from a main thrust of the second event, and associated lower-hemisphere equal-area stereoplots of the restored structures (see Figure 7 for locations). In A, note the overturned backthrust as a result of sole thrust-related simple shear.

FIGURE 9. (A) Field sketch of the highly deformed anticline core associated to the second deformation event (see Figure 7 for location). An early deformation event has been recognized in this outcrop, which consisted on bed-scale thrusting and stretching (B and C). Note the slight difference in transport direction between the two events. Legend indicates the structural elements in the stereoplots.

FIGURE 10. Folded fold exposed on the road cut at Pontedo Gorge, not visible in map view (see photograph in Figure 6H and Figure 7 for location). The fold is developed in calciturbidites and marls of facies C1 and M1. The first folding event is associated to bed-scale thrusts. Lower-hemisphere equal-area stereoplot displays the restored orientations

of the fold axial planes and axes associated to the second (solid plane and point for average axis) and third (dashed plane and hollow point for average axis) folding events. Note the dispersion in fold axes orientations of the second thrusting event, depicted as red squares. Estimated transport directions for the second (short black arrow) and third (short white arrow) events are indicated.

FIGURE 11. Restored profile of the third deformation event and lower-hemisphere equal-area stereoplots of the restored structures. Orientation is referred to the restored section. Stratigraphic top is towards top of page.

FIGURE 12. Sequential restoration of the structures exposed in the Pontedo Gorge area to the undeformed state displaying the different deformation events.

FIGURE 13. Lower-hemisphere equal-area stereoplots displaying the restored orientations of the structures measured in the Pontedo Gorge area. Arrows indicate the averaged transport direction for each plot. Note the relative dispersion in orientations. Contours represent 1% increments on the frequency of pole data. Rose diagrams are constructed so that the number of data is proportional to the area of the wedges, not to their length.

FIGURE 14. General map of the area located to the west (A) and east (B) of the Pontedo Gorge, and lower-hemisphere equal-area stereoplots of the restored structures. (A) Two listric extensional faults with associated rollover folds converge into a basal detachment that transfers displacement towards the compressive structures in the Pontedo Gorge. (B) Two listric extensional faults are present: the westernmost has associated a drag syncline and a rollover anticline, whereas the easternmost is a slump scar onlaped by lower slope-basin deposits. For legend see Figures 2 and 5.

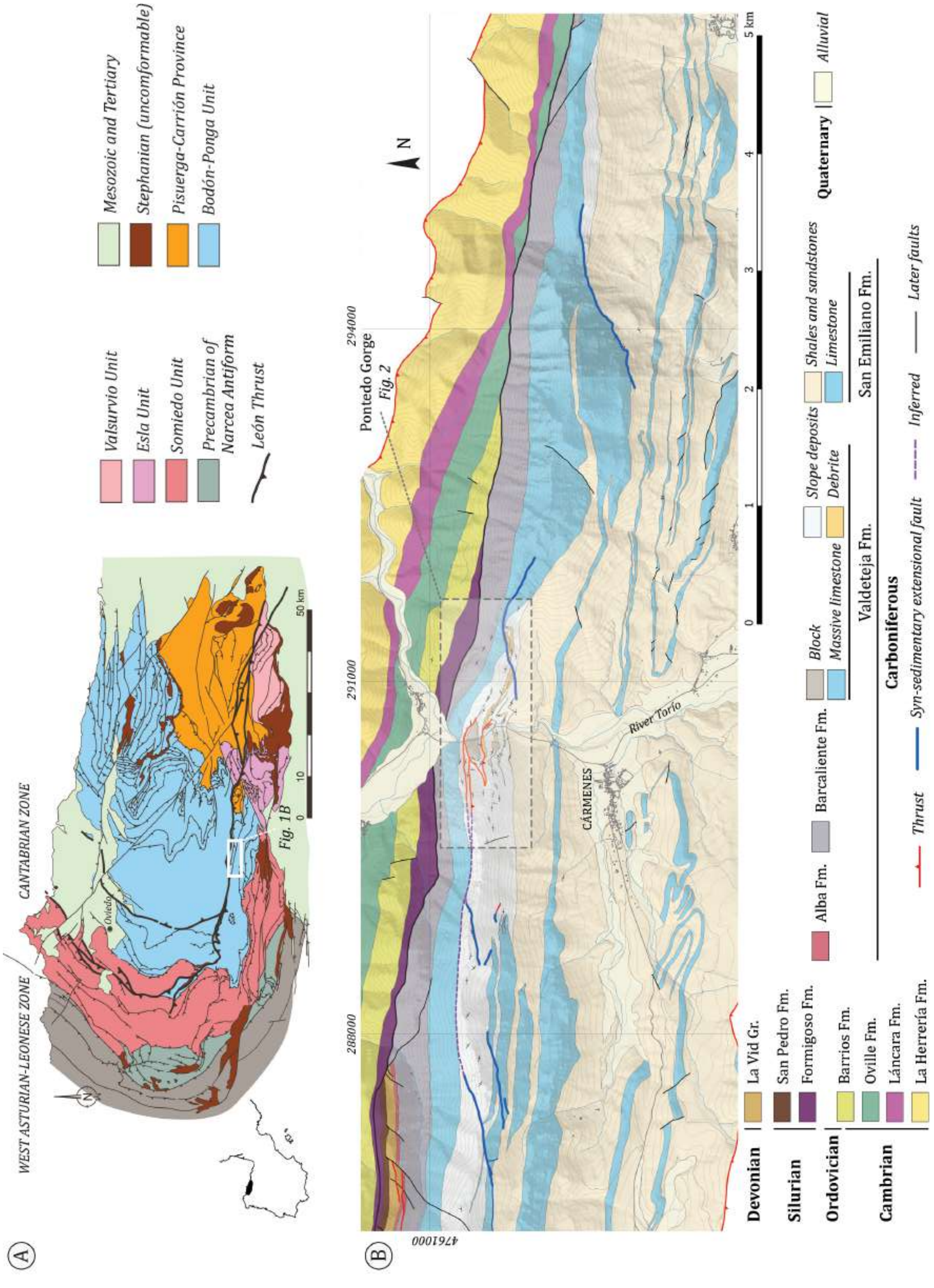

FIGURE 1. (A) Geological map of the Cantabrian Zone showing its recent-most subdivision (modified from Alonso *et al.*, 2009). (B) General map of the northernmost sector of the Bodón Nappe. Boxed area indicates the location of the Pontedo Gorge area, where a detailed map has been elaborated (Fig. 2).

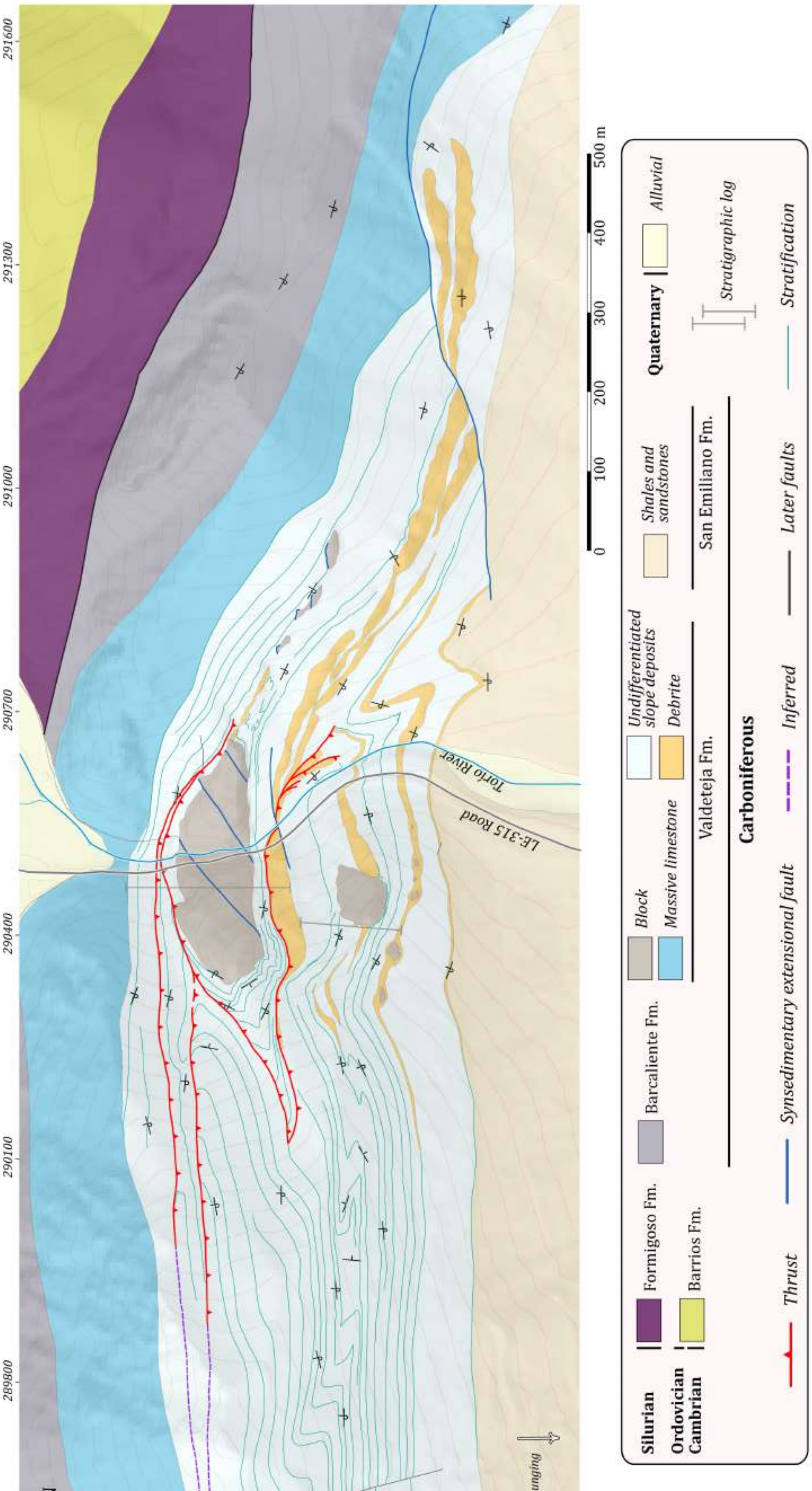

FIGURE 2. Detailed geological map of the Pontedo Gorge area.

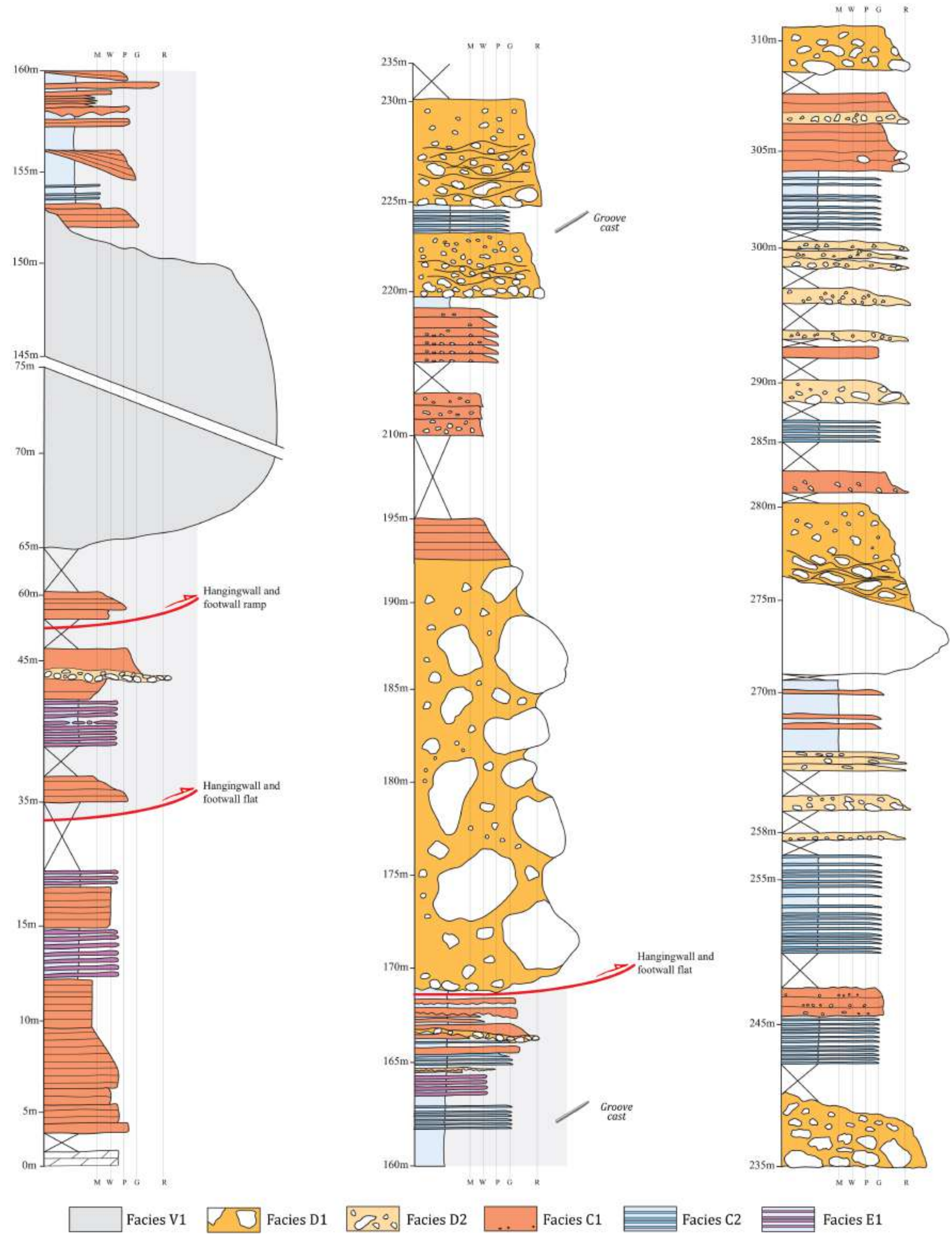

FIGURE 3. Detailed stratigraphic log of the studied interval of the Valdeteja Fm. Duplicated interval is shadowed.

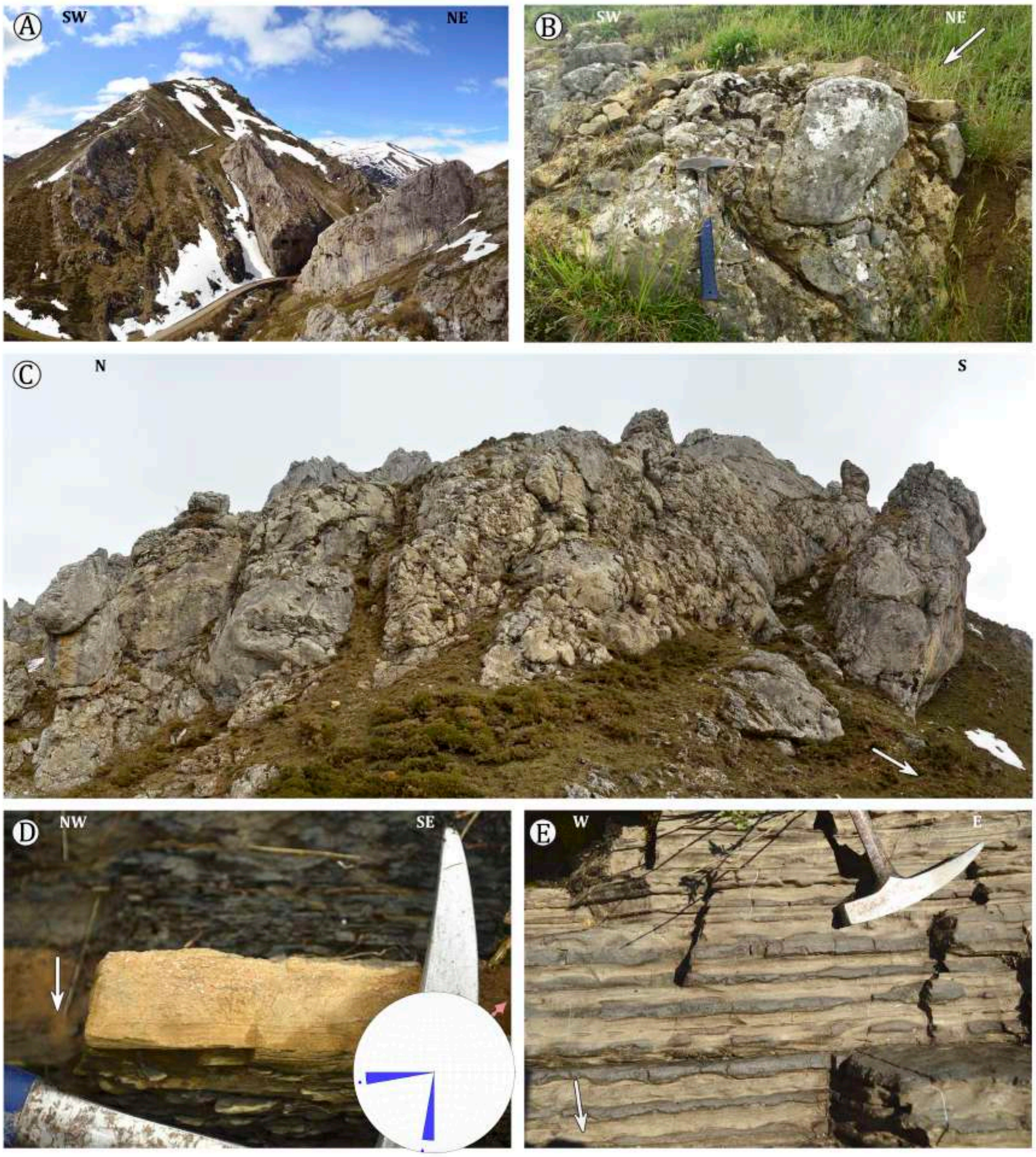

FIGURE 4. Field photographs of the sedimentary facies. Arrows indicate the top of the succession (notice it is overturned in all cases). (A) Large block (325 m) of facies V1 eroded by the Torío River. (B) Detail of facies D2. (C) Fieldwork aspect of facies D1 (cliff is *ca.* 12 m-high). (D) Facies C2 bed composed of a graded division, overlain by a laminated division and a final mudstone cap. Restored orientations of groove casts developed parallel to the paleocurrent are indicated. (E) Facies E1. Notice the nodular appearance of some beds.

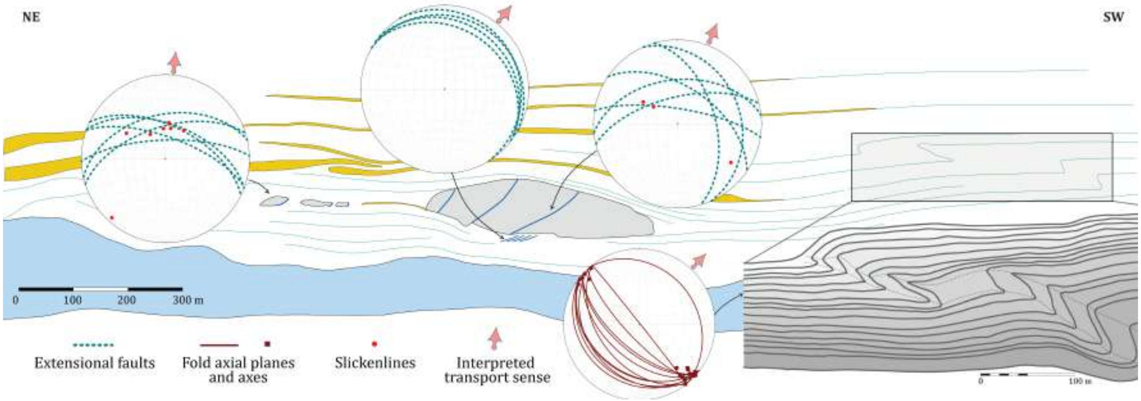

FIGURE 5. Restored profile of the first deformation event. Lower-hemisphere equal-area stereoplots of the restored structures are referred to their location with a thin black arrow. Legend indicates the structural elements in the stereoplots. Orientation is referred to the restored section. Stratigraphic top is towards top of page.

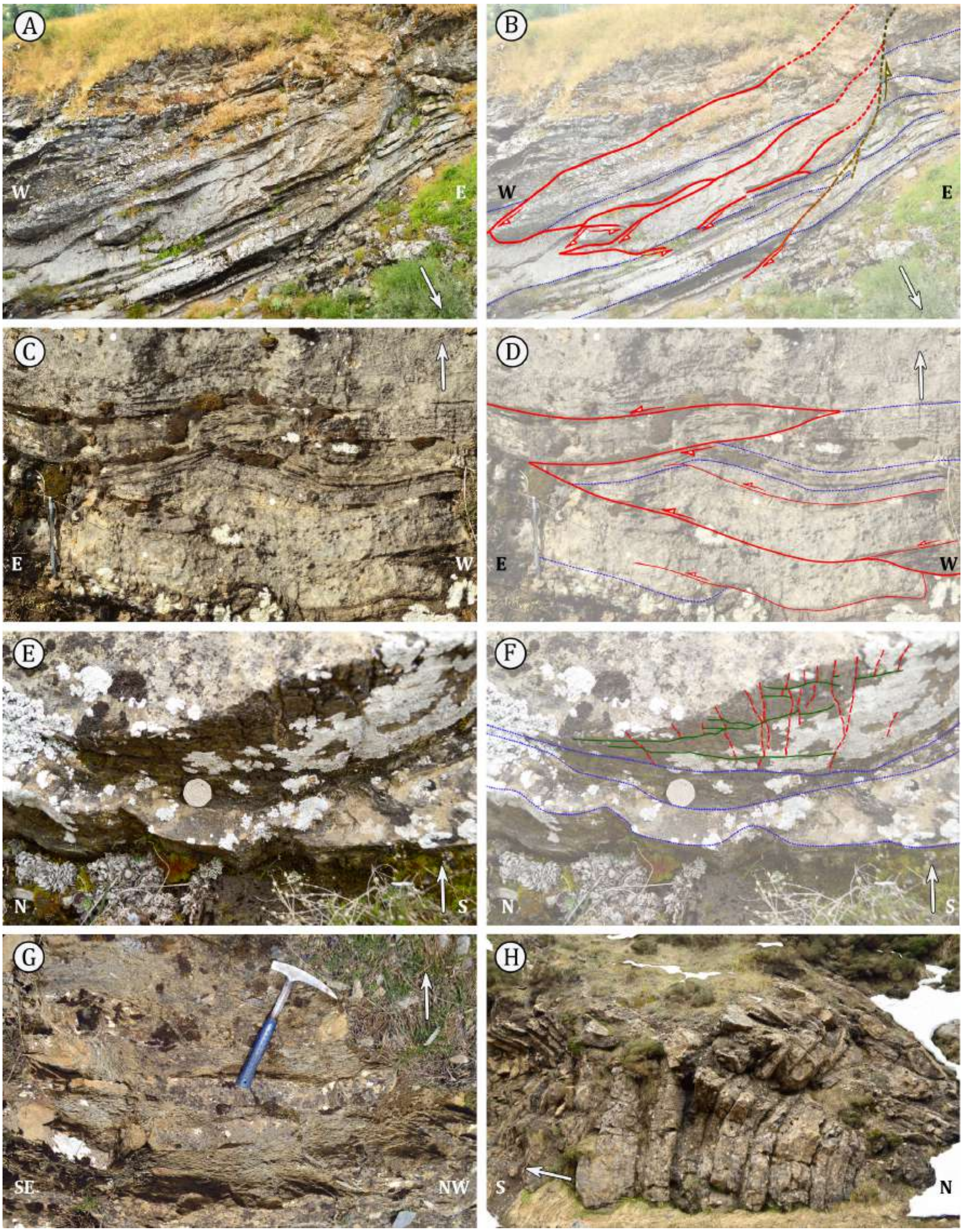

FIGURE 6. Field photographs of structural features. Arrows indicate the top of the succession. (A) Basal shear zone below the large block of facies V1, developed in facies C1 and E1. Note that the succession is overturned. (B) Interpretation of A, with red thrusts and a reactivated extensional fault (note the change in throw along the easternmost fault, normal in the lower part and reverse in the upper part). (C) Bed-scale compressional structures in facies C2 (location 3 m to the south-east from E). (D) Interpretation of C: note the development of a small-scale double thrust wedge. (E) Bed-scale extensional structures in facies C2 (see boudin necks in Figure 9 for location). (F) Interpretation of E: note the boudinage in the lower bed, and the orthogonal relation between two sets of hydroplastic fractures. The trends of red and green sets are, respectively, normal and parallel to transport sense. (G) Bed-scale view of imbricate thrusts (see Figure 8B for

interpretation). (H) Refolded fold seen in lateral view in a road cut (see Figure 10 for interpretation).

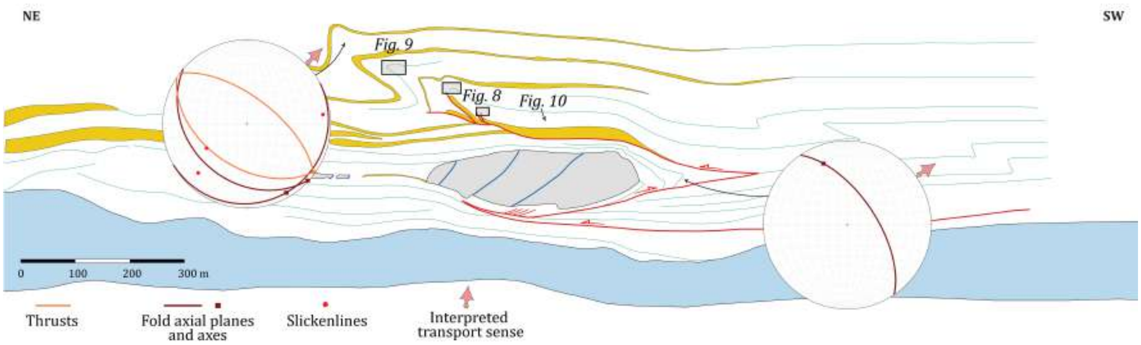

FIGURE 7. Restored profile of the second deformation event and lower-hemisphere equal-area stereoplots of the restored structures. Location of figures 8 and 9 (subparallel sections to the profile) and 10 (lateral view, at high angle to the profile) is indicated. Orientation is referred to the restored section. Stratigraphic top is towards top of page.

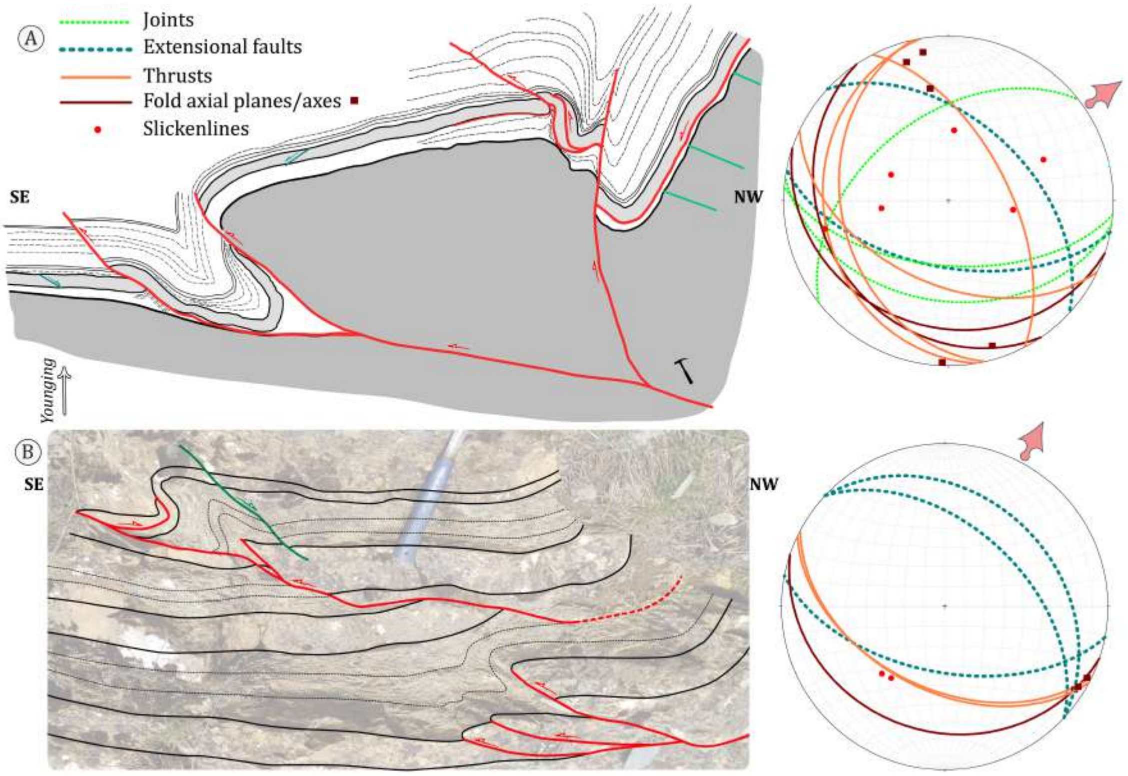

FIGURE 8. Detailed map (A) and interpreted photograph (B, see Figure 6G) of locations in the imbricate thrusts branched from a main thrust of the second event, and associated lower-hemisphere equal-area stereoplots of the restored structures (see Figure 7 for locations). In A, note the overturned backthrust as a result of sole thrust-related simple shear.

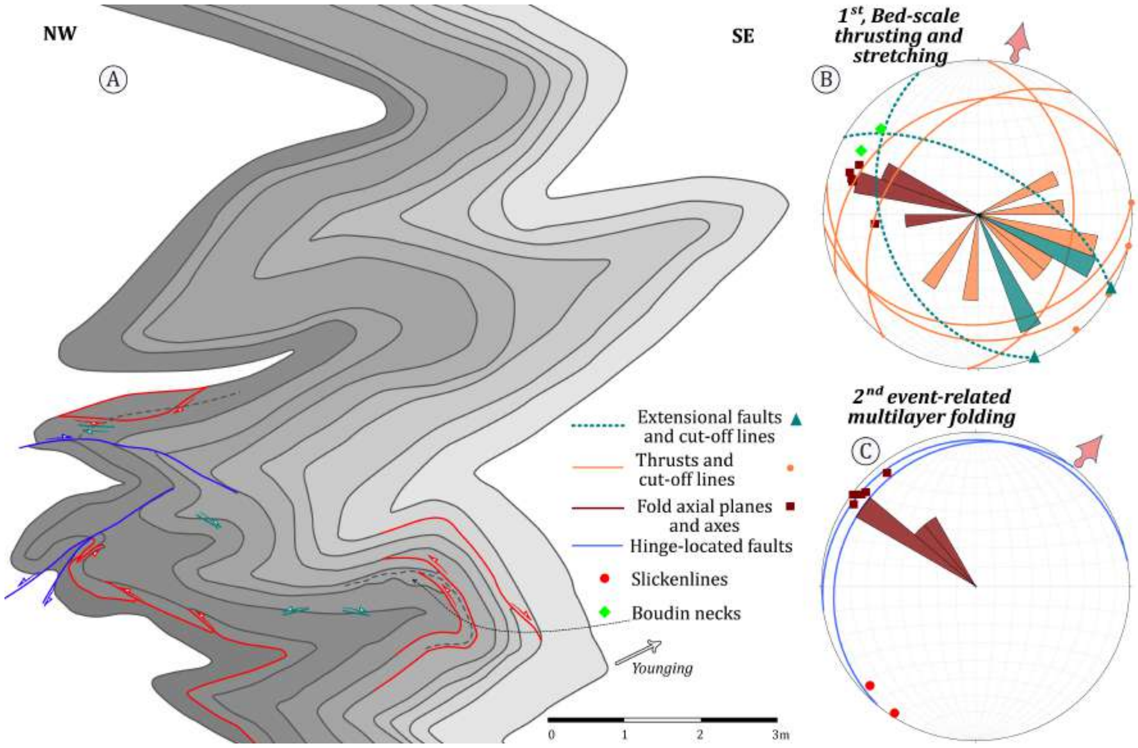

FIGURE 9. (A) Field sketch of the highly deformed anticline core associated to the second deformation event (see Figure 7 for location). An early deformation event has been recognized in this outcrop, which consisted on bed-scale thrusting and stretching (B and C). Note the slight difference in transport direction between the two events. Legend indicates the structural elements in the stereoplots.

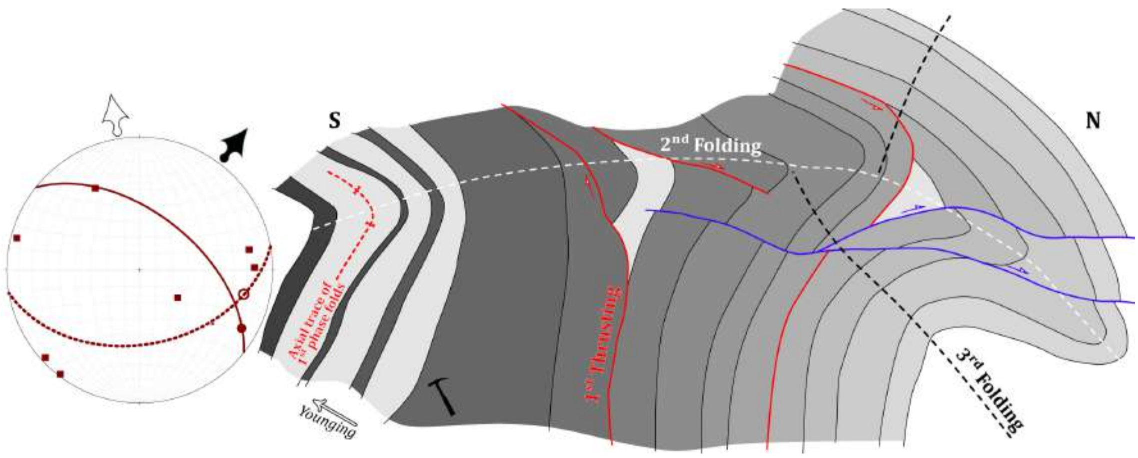

FIGURE 10. Folded fold exposed on the road cut at Pontedo Gorge, not visible in map view (see photograph in Figure 6H and Figure 7 for location). The fold is developed in calciturbidites and marls of facies C1 and M1. The first folding event is associated to bed-scale thrusts. Lower-hemisphere equal-area stereoplot displays the restored orientations of the fold axial planes and axes associated to the second (solid plane and point for average axis) and third (dashed plane and hollow point for average axis) folding events. Note the dispersion in fold axes orientations of the second thrusting event, depicted as red squares. Estimated transport directions for the second (short black arrow) and third (short white arrow) events are indicated.

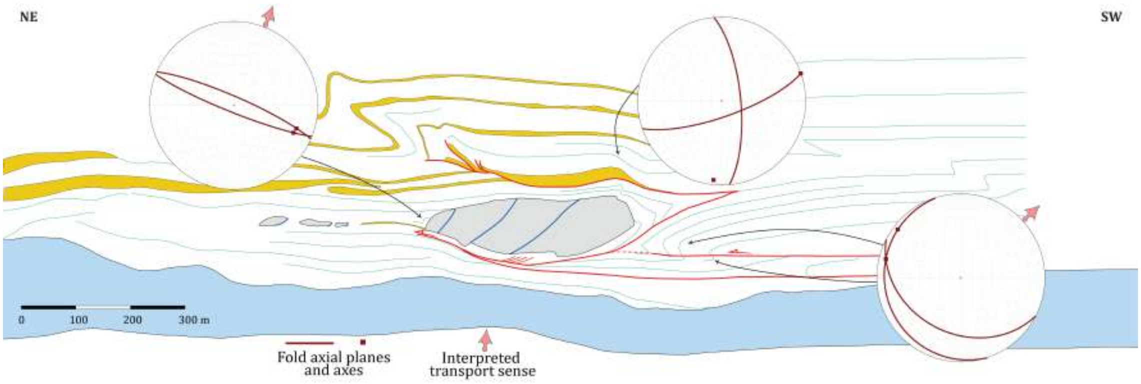

FIGURE 11. Restored profile of the third deformation event and lower-hemisphere equal-area stereoplots of the restored structures. Orientation is referred to the restored section. Stratigraphic top is towards top of page.

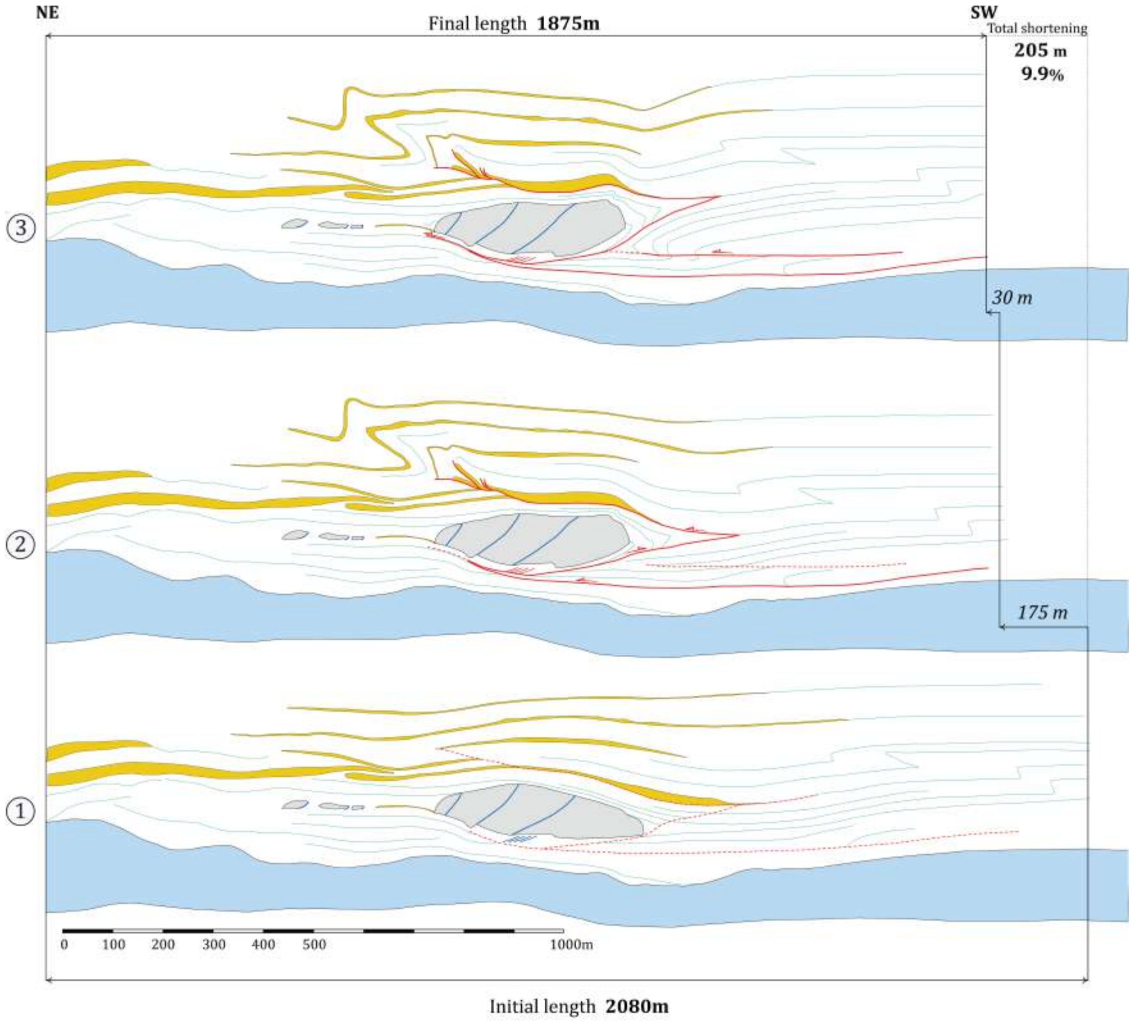

FIGURE 12. Sequential restoration of the structures exposed in the Pontedo Gorge area to the undeformed state displaying the different deformation events.

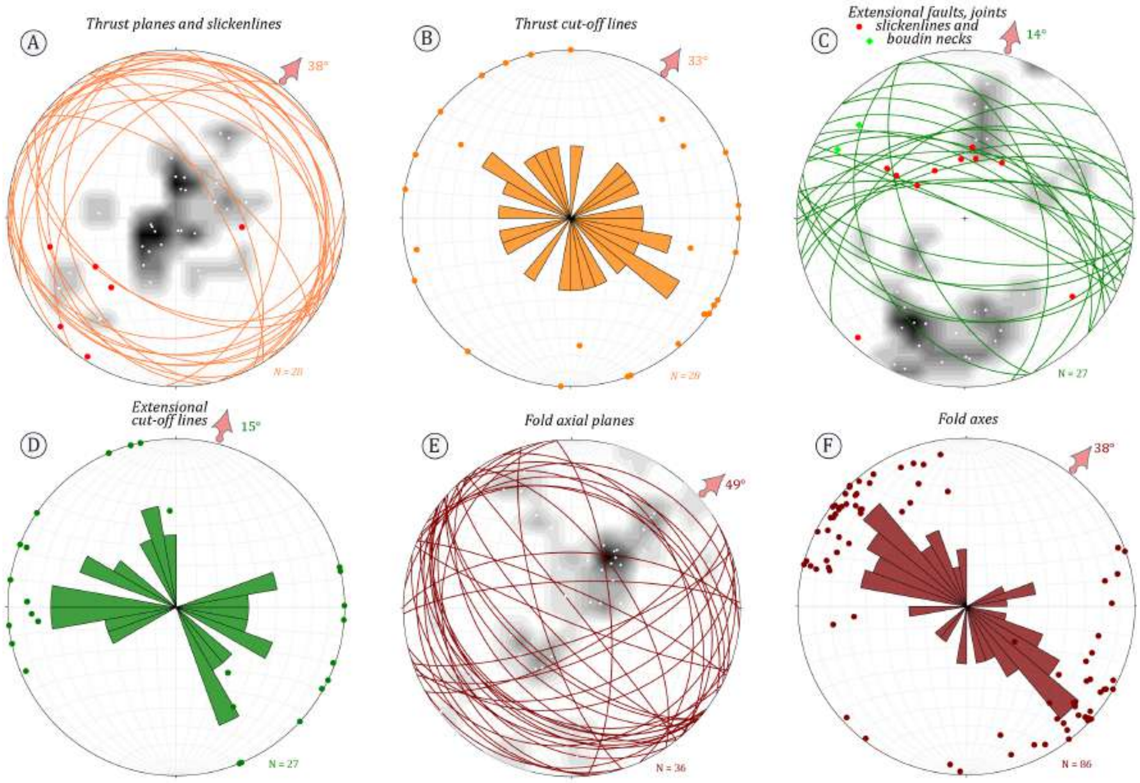

FIGURE 13. Lower-hemisphere equal-area stereoplots displaying the restored orientations of the structures measured in the Pontedo Gorge area. Arrows indicate the averaged transport direction for each plot. Note the relative dispersion in orientations. Contours represent 1% increments on the frequency of pole data. Rose diagrams are constructed so that the number of data is proportional to the area of the wedges, not to their length.

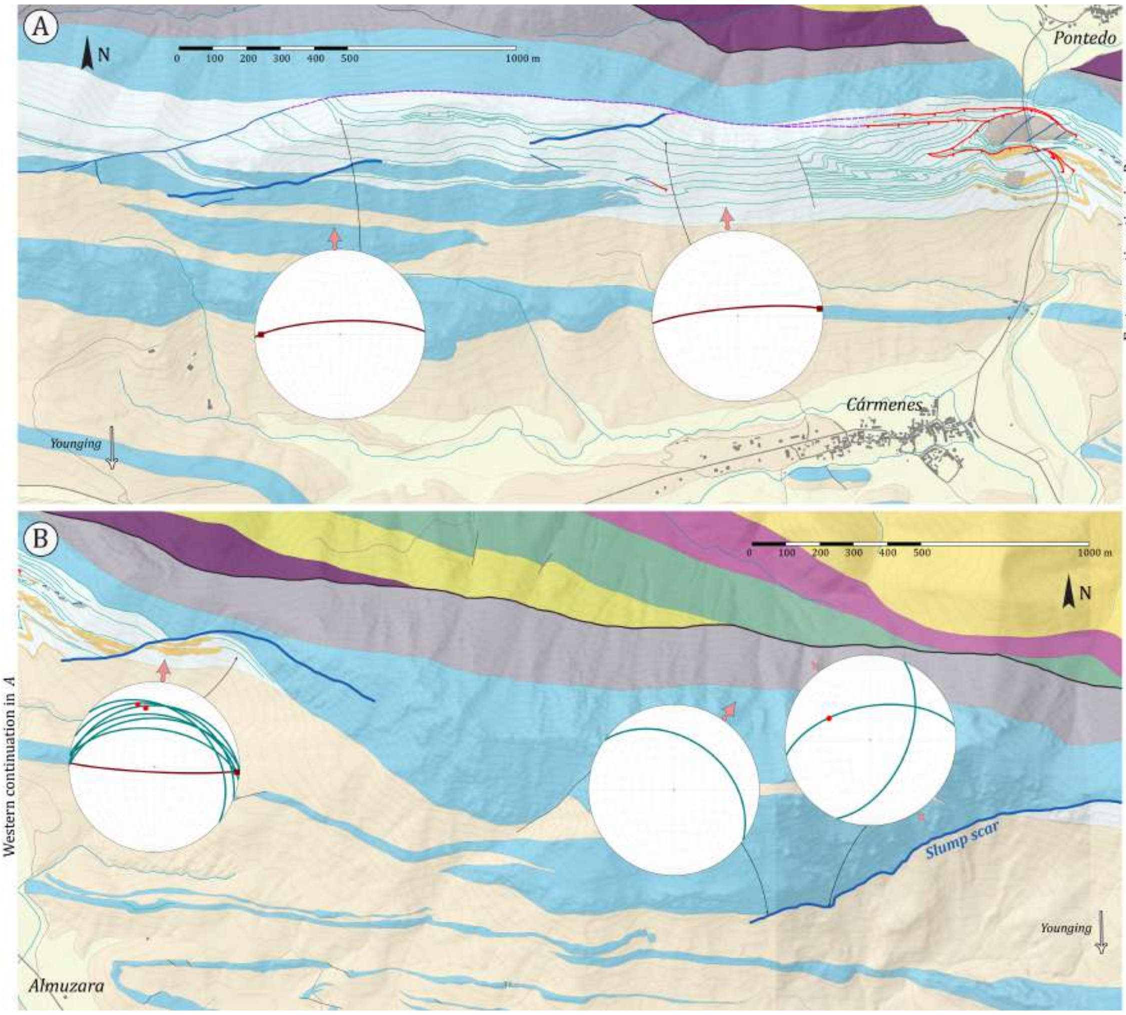

FIGURE 14. General map of the area located to the west (A) and east (B) of the Pontedo Gorge, and lower-hemisphere equal-area stereoplots of the restored structures. (A) Two listric extensional faults with associated rollover folds converge into a basal detachment that transfers displacement towards the compressive structures in the Pontedo Gorge. (B) Two listric extensional faults are present: the westernmost has associated a drag syncline and a rollover anticline, whereas the easternmost is a slump scar onlaped by lower slope-basin deposits. For legend see Figures 2 and 5.